

Published in final edited form as:

Nature. 2020 July 01; 583(7816): 447–452. doi:10.1038/s41586-020-2296-7.

A distal enhancer at risk locus 11q13.5 promotes suppression of colitis by Treg cells

Rabab Nasrallah^{#1}, Charlotte J. Imianowski^{#1,2}, Lara Bossini-Castillo³, Francis M. Grant¹, Mikail Dogan⁴, Lindsey Placek⁴, Lina Kozhaya⁴, Paula Kuo^{1,2}, Firas Sadiyah^{1,2}, Sarah K. Whiteside^{1,2}, Maxwell R. Mumbach⁵, Dafni Glinos³, Panagiota Vardaka^{1,2}, Carly E. Whyte¹, Teresa Lozano¹, Toshitsugu Fujita^{6,7}, Hodaka Fujii^{6,7}, Adrian Liston¹, Simon Andrews⁸, Adeline Cozzani⁹, Jie Yang^{1,2}, Suman Mitra⁹, Enrico Lugli¹⁰, Howard Y Chang⁵, Derya Unutma⁴, Gosia Trynka^{3,11}, Rahul Roychoudhuri^{1,2}

¹Laboratory of Lymphocyte Signalling and Development, The Babraham Institute, Cambridge, UK

²Department of Pathology, University of Cambridge, Cambridge, UK

³Immune Genomics Group, Wellcome Sanger Institute, Cambridge, UK

⁴The Jackson Laboratory, Farmington, CT, USA

⁵Howard Hughes Medical Institute and Center for Personal Dynamic Regulomes, Stanford University School of Medicine, Stanford, California, USA

⁶Chromatin Biochemistry Research Group, Research Institute for Microbial Diseases, Osaka University, Osaka, Japan

⁷Department of Biochemistry and Genome Biology, Hirosaki University Graduate School of Medicine, Hirosaki, Japan

⁸Bioinformatics Group, The Babraham Institute, Cambridge, UK

⁹The University of Lille and Inserm UMR1277 CNRS UMR9020 – CANTHER and Institut pour la Recherche sur le Cancer de Lille, France

¹⁰Humanitas Clinical and Research Center, Milan, Italy

¹¹Open Targets, Wellcome Genome Campus, Cambridge, UK

These authors contributed equally to this work.

Abstract

Correspondence to: Charlotte J. Imianowski; Gosia Trynka; Rahul Roychoudhuri.

Correspondence and requests for materials should be addressed to R.R. (rr257@cam.ac.uk), C.J.I (cji27@cam.ac.uk) and G.T. (gosia@sanger.ac.uk).

Author contributions

R.N., C.J.I., F.M.G., M.D., L.P., L.K., P.K., F.S., S.K.W., A.C., P.V., C.E.W., T.L., T.F., C.N., H.F., E.L., D.U., S.M. and R.R. performed experiments. L.B.C., D.G. and G.T. performed and analysed hQTL and eQTL analyses of human T cells. R.N., C.J.I., F.S., M.R.M., H.F., J.Y., A.L., S.A., G.T. and R.R. analysed data. R.N., C.J.I., L.B.C., G.T. and R.R. wrote the manuscript. H.Y.C., D.U., G.T. and R.R. provided overall supervision of the work.

Author information

Reprints and permissions information is available at www.nature.com/reprints.

The authors have no competing interests to declare.

Genetic variations underlying susceptibility to complex autoimmune and allergic diseases are concentrated within non-coding regulatory elements termed enhancers¹. The functions of a vast majority of disease-associated enhancers are unresolved, in part due to their distance from genes they regulate, a lack of understanding of the cell types in which they operate, and our inability to recapitulate the biology of immune diseases *in vitro*. Here, using shared synteny to guide loss-of-function analysis of human enhancer homologs in mice, we show that the prominent autoimmune/allergic disease risk locus at chromosome 11q13.5^{2–7} contains a distal enhancer commissioned in CD4⁺ regulatory T (T_{reg}) cells and required for T_{reg}-mediated suppression of colitis. The enhancer recruits transcription factors STAT5 and NF-κB to mediate signal-driven expression of *Lrrc32*, encoding Glycoprotein A Repetitions Predominant (GARP). Whereas disruption of the *Lrrc32* gene results in early lethality, mice lacking the enhancer are viable but lack GARP expression on Foxp3⁺ T_{reg} cells, which are unable to control colitis. In human T_{reg} cells, the enhancer forms conformational interactions with the promoter of *LRRC32* and enhancer risk variants are associated with reduced histone acetylation and GARP expression. Finally, functional fine-mapping of 11q13.5 identifies a single CRISPRa-responsive element in the vicinity of risk variant rs11236797 capable of driving GARP expression. These findings provide a mechanistic basis for association of the 11q13.5 risk locus with immune-mediated diseases and identify GARP as a potential target in their therapy.

Genetic polymorphisms at human chromosome 11q13.5 are associated with susceptibility to Crohn's disease and ulcerative colitis^{2,3}, type I diabetes⁴, asthma^{5,6}, allergic rhinitis⁶ and atopic dermatitis^{6,7}. The molecular basis for this association is unresolved. Imputation of linkage disequilibrium (LD) at 11q13.5 revealed a cluster of highly linked variants associated with immune disease occupying an intergenic region not containing the promoters of known protein-coding genes (Fig. 1a and Extended Data 1). Lymphocytes play a critical role in immune disease. Examination of histone modifications within multiple primary lymphocyte lineages revealed enrichment of H3K27Ac at the identified locus within CD4⁺ CD127[−] CD25⁺ T_{reg} cells compared with other lineages examined (Fig. 1b and Extended Data 2)⁸, suggesting the presence of a distal enhancer at 11q13.5 active within T_{reg} cells.

Whereas conventional T (T_{conv}) cells promote immune activation and can drive immune-mediated pathology, T_{reg} cells suppress their function to maintain immune homeostasis^{9,10}. T_{reg} cells, dependent upon the transcription factor Foxp3, exert multiple biological functions that are poorly recapitulated *in vitro*. In order to better understand the function of the identified locus, we asked whether a homologous region in mice is amenable to loss-of-function analysis *in vivo*. Analysis of shared synteny between human and mouse genomes identified a region of mouse chromosome 7 homologous to the identified locus in humans (Fig. 1c-d and Supplementary Table 1). This region was accessible in mouse T_{reg} cells and enriched in H3K4me1 and H3K27Ac (Fig. 1e), consistent with the presence of a distal enhancer¹¹. We generated knockout mice (hereinafter Enh-KO mice) lacking a 2.3 kb region homologous to the human risk locus (Chr7:105,711,382-105,713,753; 71% sequence identity) using CRISPR-based mutagenesis. Enh-KO mice exhibited similar body mass and survival to wildtype (WT) littermates (Extended Data 3a–b). The phenotype of T cells in the thymus and periphery were similar between WT and Enh-KO animals (Extended Data 3c–f).

This suggested that the identified enhancer is not required to maintain immune homeostasis under basal conditions

Susceptibility to complex diseases is a product of genetic and environmental factors. Given the association of 11q13.5 polymorphisms with ulcerative colitis and Crohn's disease^{2,3}, we tested the susceptibility of Enh-KO animals to colitis driven by dextran sulphate sodium, the severity of which is affected by T_{reg} cells^{12,13}. Enh-KO mice were more susceptible to DSS-induced colitis, as indicated by increased weight loss (Fig. 1f), reduction in colon length (Extended Data 4a) and induction of macroscopic and histopathological features of colitis (Fig. 1g–h and Extended Data 4b–c). Greater frequencies of CD4⁺ T_{conv} cells within the colonic lamina propria and mLN of DSS-treated Enh-KO animals expressed interferon (IFN)- γ whereas there were no differences in the frequency of Foxp3⁺ T_{reg} cells (Fig. 1i and Extended Data 5a). This coincided with increased concentrations of IFN- γ , tumour necrosis factor (TNF)- α and interleukin (IL)-6 in sera of DSS-treated Enh-KO animals (Fig. 1j and Extended Data 5bx2013;c). By contrast, we noted similar levels of C-X-C motif ligand 1 (CXCL1) and IL-10 in sera of WT and Enh-KO animals (Extended Data 5d–e). Collectively, these results indicate that the identified enhancer is required to maintain gut immune homeostasis in the face of extrinsic colitogenic stimuli.

Since the identified region contained active enhancer marks in Foxp3⁺ T_{reg} cells, we asked whether it regulates gene expression within these cells. We subjected CD4⁺ T_{reg} and T_{conv} cells isolated by FACS from WT and Enh-KO *Foxp3*^{EGFP} reporter animals to massively parallel RNA sequencing (RNA-Seq). Whereas enhancer loss did not significantly affect gene expression within T_{conv} cells, its loss within T_{reg} cells resulted in a ~36-fold reduction in the expression of the *Lrrc32* gene, which encodes the protein GARP (Fig. 2a and Supplementary Table 2). Moreover, the enhancer is required for the maintenance of local accessible chromatin but not the broader landscape of accessible elements (Extended Data 6a–b).

GARP is a 72 kDa transmembrane glycoprotein expressed by T_{reg} cells, platelets, endothelial cells and lipopolysaccharide (LPS)-activated B cells^{14–19}. GARP binds latent TGF- β on the cell surface which is cleaved by integrin α V β 8 to cause local release of active TGF- β . Consistent with reduced *Lrrc32* expression by T_{reg} cells from Enh-KO animals, flow cytometry analysis revealed striking reduction in expression of GARP on the surface of Foxp3⁺ T_{reg} cells in the spleen, thymus and mesenteric lymph nodes (mLN) of Enh-KO animals (Fig. 2b and Extended Data 6c–d). By contrast, GARP expression was not substantially reduced on Enh-KO naïve or memory CD4⁺ T_{conv} cells isolated *ex vivo* (Fig. 2c and Extended Data 7a) or T_{conv} cells stimulated briefly *in vitro* (Extended Data 7b). Consistently, we noted the presence of acetylated histones at the identified enhancer in resting and activated T_{reg} cells that was Foxp3-dependent and reduced in naïve and effector CD4⁺ T_{conv} cells (Extended Data 7c)²⁰. Additionally, the enhancer was not required for GARP expression on other cells known to express GARP, including lung endothelial cells, activated platelets and LPS-activated B cells (Fig. 2d and Extended Data 8a–b), and did not regulate GARP expression on a variety of other splenic non-T_{reg} cell types (Extended Data 8c–e). Consistent with tissue-specificity in the function of the enhancer, whereas homozygous disruption of the *Lrrc32* gene resulted in complete early lethality, viable

progeny homozygous for deletion of the enhancer (hereinafter *Lrrc32*+70k) were obtained at expected Mendelian ratios (Fig 2e).

We noted the presence of highly conserved Signal Transducer and Activator of Transcription 5 (STAT5) and Nuclear Factor κ -light-chain-enhancer of Activated B cells (NF- κ B) binding motifs within *Lrrc32*+70k, which play canonical roles in IL-2 and TCR-driven gene expression, respectively (Extended Data 9a). We asked whether these transcription factors bind *Lrrc32*+70k to mediate signal-driven GARP expression on T_{reg} cells. We found that STAT5 was recruited to *Lrrc32*+70k in response to brief (1h) IL-2 stimulation of *in vitro*-derived induced T_{reg} (iT_{reg}) cells (Fig. 2f). Correspondingly, we noted STAT5 binding at the homologous enhancer in human T_{reg} cells but not T_{conv} cells (Extended Data 9b)²¹. Analysis of known NF- κ B p65 binding activity also revealed TCR-driven NF- κ B p65 binding to *Lrrc32*+70k within T_{reg} cells but not T_{conv} cells in response to TCR stimulation (Fig. 2g)²². Consistent with its ability to bind signal-dependent TFs, *Lrrc32*+70k was absolutely required for IL-2-driven GARP expression on T_{reg} cells, whereas TCR-driven GARP expression was only partially enhancer-dependent (Fig. 2h and Extended Data 9c). IL-2-driven GARP expression was abrogated by pre-treatment of cells with the janus kinase (JAK) inhibitor, Tofacitinib, which inhibits signal-driven activation of STAT TFs (Fig. 2i)²³. Similarly, GARP induction driven by TCR stimulation was partially blocked by pre-treatment of cells with BI 605906, a highly specific inhibitor of the protein kinase IKK β whose activity is required for canonical NF- κ B activation (Fig. 2j). This result is consistent with prior RNA-Seq analyses of WT and *Rela*^{-/-} *Rel*^{-/-} T_{reg} cells which demonstrated markedly decreased stimulation-driven expression of *Lrrc32* mRNA in the absence of canonical NF- κ B signalling²². Collectively, these data demonstrate that *Lrrc32*+70k binds to STAT5 and NF- κ B in response to IL-2 and TCR signalling and functions as a regulatory node for signal-driven GARP expression on T_{reg} cells.

Because Enh-KO animals exhibited increased susceptibility to colitis, we asked whether T_{reg} cells from Enh-KO animals are defective in their ability to control gut inflammation. GARP is dispensable for the suppressive function of mouse T_{reg} cells as measured *in vitro*²⁴, but is required for optimal suppressive function *in vivo*^{25,26}. To test the function of Enh-KO T_{reg} cells *in vivo*, we reconstituted *Rag2*-deficient animals with 4x10⁵ CD4⁺ naïve T (T_{nai}) cells from wildtype mice, alone or in combination with 1x10⁵ WT or Enh-KO T_{reg} cells. Whereas weight loss and induction of clinical features colitis caused by transfer of naïve T cells were reduced by the co-transfer of WT T_{reg} cells, T_{reg} cells from Enh-KO animals were insufficient in suppressing colitis (Fig. 3a–b). Distinguishing transferred CD45.2⁻ T_{conv} cells from CD45.2⁺ T_{reg} cells, we found Enh-KO T_{reg} cells accumulated to higher frequencies than WT T_{reg} cells within mLN of recipient mice (Extended Data 9d) but expressed substantially reduced GARP in both mLN and spleen (Fig. 3c and Extended Data 9e). Consistent with their inability to adequately constrain colitis, we observed increased effector cytokine expression by CD45.2⁻ T_{conv} cells among animals that received Enh-KO T_{reg} cells (Fig. 3d and Extended Data 9f). Collectively, these data indicate that *Lrrc32*+70k is required for T_{reg}-mediated suppression of colitis *in vivo*.

We asked whether genetic variations at 11q13.5 affect enhancer function in human T_{reg} cells. CD4⁺CD127⁻CD25⁺ T_{reg} cells were sorted by FACS from peripheral blood of

genotyped healthy donors and H3K27Ac enrichment was measured. We found that a cluster of linked 11q13.5 variants were associated with differential enhancer acetylation in human T_{reg} cells (Fig. 4a–b and Supplementary Tables 3–4)²⁷. Strikingly, there was significant co-localisation between variants associated with differential acetylation and those associated with IBD risk (Fig. 4c and Supplementary Table 5). Reciprocal virtual 4C (v4C) analysis of previously generated H3K27Ac HiChIP interaction maps²⁸ revealed significant interactions between the identified enhancer and the *LRRC32* promoter within human T_{reg} but not naïve or Th17 cells (Fig. 4d), contained within a sub-topologically associated domain previously mapped within a human lymphoid line²⁹ (Extended Data 10a–b). To test the effect of 11q13.5 polymorphisms on *LRRC32* expression, CD4⁺ CD127⁻ CD25⁺ T_{reg} cells were sorted by FACS from peripheral blood of genotyped healthy donors and *LRRC32* expression was determined using RNA-Seq. This analysis revealed that 11q13.5 polymorphisms were nominally associated with differential *LRRC32* mRNA expression under basal conditions (Extended Data 10c). Moreover, rs11236797 polymorphisms were significantly associated with both basal and stimulation-driven GARP expression on CD4⁺CD127⁻CD25⁺ T_{reg} cells (Fig. 4e). Thus, disease-associated genetic polymorphisms within 11q13.5 affect enhancer histone acetylation and GARP expression on human T_{reg} cells.

Since risk variants at 11q13.5 are in high LD, we performed a CRISPR activation (CRISPRa) screen to enable fine-mapping of candidate stimulation-responsive enhancers and causal variants within 11q13.5³⁰. sgRNA target sequences in proximity to risk variants within 11q13.5 were subcloned into lentiviral vectors and individually co-expressed with VP64-dCas9/GFP and activator helper complex MS2-P65-HSF1 in primary *in vitro* stimulated human CD4⁺ T cells (Supplementary Table 6). Expression of GARP on the surface of GFP⁺ (transduced) cells was measured. Of 14 sgRNAs tested, three sgRNAs in the proximity of rs11236797 strongly induced GARP expression (Fig. 4f), indicating the presence of a CRISPRa-responsive element in the vicinity of risk variant rs11236797 with the capacity to drive GARP expression.

Genome-wide association studies have provided insights into the genetic architecture of human immune-mediated disease. However, it has been difficult in many cases to infer the cell types underlying disease pathophysiology. In this study, we find that the prominent autoimmune/allergic disease risk locus at human chromosome 11q13.5 contains a distal enhancer required to control signal-driven expression of GARP by T_{reg} cells. Using shared synteny to guide loss-of-function analysis of the homologous enhancer in mice, we find that this function is required to promote T_{reg}-mediated suppression of colitis. These findings provide a basis for association of 11q13.5 polymorphisms with susceptibility to complex autoimmune and allergic diseases and identify GARP as a potential target in their therapy.

Methods

Mice and Reagents

Animals were housed at the Babraham Institute Biological Services Unit and experiments were conducted with the approval of the UK Home Office and the Babraham Institute Animal Welfare and Ethical Review Body and complied with all relevant ethical regulations. *Lrrc32*+70k Enh-KO mice were generated as described below, and were crossed to

Foxp3^{GFP} mice (C.Cg-Foxp3tm2Tch/J; Jackson laboratories) to generate WT and Enh-KO *Foxp3*^{GFP} reporter animals. *Rag2*-deficient animals used as hosts for T cell transfer colitis experiments (B6 (Cg)-Rag2tm1.1Cgn/J) were originally obtained from Jackson laboratories and maintained at the Babraham Institute. *Lrrc32*^{-/-} mice have been described previously¹. Littermate controls or age- and sex-matched animals on a C57BL/6 background were used as indicated. Mendelian ratios of early viability were calculated by assessing the genotypes of all progeny surviving to 2 weeks of age resulting from heterozygous Enh-KO or *Lrrc32*-knockout crosses.

Generation of *Lrrc32* +70k Enh-KO mice

sgRNAs containing the target sequences gRNA1 (AATGAAG GATGGCGCCA CGCTGG) and gRNA2 (TTACTCA CCACCACC ACAAGAGG) and Cas9 mRNA were generated by *in vitro* transcription and co-injected into fertilized C57BL/6 oocytes which were transferred into pseudopregnant females. The genomic region surrounding the targeted locus was amplified from genomic DNA of resultant founder progeny by polymerase chain reaction (PCR) using the following primers: 5'-TTATTCTT GGGAACAGG GGCATG-3' and 5'-AGAGGCT ACTTTGTTAC TTGGTCCC-3' and amplicons were sequenced using the following forward primer: 5'-CAATCTG TCACCTATCA GCAACGT-3'. Founder progeny bearing a 2372bp deletion corresponding to base pairs 105711382-105713753 of chromosome 7 (NCBI37/mm9), the centre of which is 69,836 bp downstream of the transcriptional start site (TSS) of *Lrrc32*, were mated with wildtype C57BL/6 animals to generate heterozygous F1 animals which were subsequently intercrossed to generate WT and Enh-KO littermate progeny.

Flow cytometry analysis of primary tissues

Single-cell suspensions from lymphoid tissues were prepared by dissociating tissues over 40µm cell strainers. Lungs were minced in media containing 20 µg/ml DNase I (Roche) and 1 mg/ml collagenase (Sigma-Aldrich) and incubated with agitation at 37 °C for 30 minutes.

Blood from tail veins or terminal cardiac bleeds were isolated in EDTA Microvette tubes (Sarstedt). Erythrocytes were lysed using ice cold ACK Lysing Buffer (Gibco) for 45 seconds. Cells requiring intracellular staining of cytokines prior to flow cytometry analysis were stimulated using phorbol 12-myristate 13-acetate (PMA), ionomycin and brefeldin A (BFA) for 4-6h in complete media. Viable cells were discriminated by staining with Zombie UV live/dead dye (Biolegend) or eFluor 780 live/dead dye (eBioscience) according to manufacturer instructions. Cells were then incubated with specific antibodies for 30 min on ice in the presence of monoclonal antibodies to block FcγR binding (anti-CD16/32 clone 2.4G2 Cat #BE0307). For intracellular staining, the eBioscience Foxp3 / Transcription Factor Staining Buffer Set (Invitrogen) was used in accordance with the manufacturer's instructions followed by intracellular staining with fluorochrome-conjugated antibodies.

The following fluorochrome-conjugated antibodies against mouse surface and intracellular antigens were used: anti-GARP (clone YGIC86, eBioscience Cat #12-9891-82), anti-FoxP3 (clone FJK-16s, eBioscience Cat #17-5773-82), anti-CD45.2 (clone 104, eBioscience Cat #69-0454-82), anti-TNF (clone MP-XT22, eBioscience Cat #25-7321-82), anti-IFN-γ

(clone XMG1.2, eBioscience Cat #45-7311-82), anti-GL7 (clone GL7, BioLegend Cat #144604), anti-CD25 (clone PC61, Becton Dickinson Cat #564023), anti-CD4 (clone RM4-5, eBioscience Cat #48-0042-82), anti-CD62L (clone MEL-14 BioLegend, Cat #104441), anti-CD44 (clone IM7, eBioscience Cat #55313), anti-CD8a (clone 53-6.7, BD Horizon Cat #563786), anti-CD19 (clone eBio1D3, eBioscience Cat #17-0193-80), anti-B220 (clone RA3-6B2, eBioscience Cat #103236). The following fluorochrome-conjugated antibodies against human surface and intracellular antigens were used: anti-CD3 (clone UCHT1, BD Horizon Cat# 563546), anti-CD4 (clone SK3, BioLegend Cat# 344608), anti-CD127 (clone A019D5, BioLegend Cat# 351320), anti-CD25 (clone BC96, BioLegend Cat# 302632), anti-GARP (clone G14D9, eBioscience Cat# 12-9882-42). Data were acquired using BD Fortessa or LSRII flow cytometers and analysed using FlowJo (TreeStar).

For high parameter flow cytometry, cells were incubated on ice for 30 minutes in the presence of 2.4G2 monoclonal antibodies to block Fc γ R binding. Cells were then stained with Fixable Viability Dye eFlour 780 and antibodies against surface antigens, followed by fixation with 2% formaldehyde and staining with antibodies against intracellular antigens. Antibodies used were anti- $\gamma\delta$ -TCR clone GL3 (eBioscience), anti-CD11b clone M1/70 (eBioscience), anti-CD90.2 clone 53-2.1 (Biolegend), anti-CD11c clone N418 (Biolegend), anti-Ly6G clone 1A8 (Biolegend), anti-Ly6C clone HK1.4 (Biolegend), anti-Foxp3 clone FJK-16s (eBioscience), anti-Siglec F clone E50-2440 (BD Biosciences), anti-TCR β clone H57-597 (BD Bioscience), anti-GARP clone YGIC86 (eBioscience), anti-F4/80 clone BM8 (eBioscience), anti-NK1.1 clone PK136 (Biolegend), anti-CD3 clone 145-2C11 (eBioscience), anti-CD45 clone 30-F11 (BD Biosciences), anti-CD4 clone GK1.5 (BD Biosciences), anti-CD19 clone 1D3 (BD Biosciences), anti-PDCA-1 clone 927 (BD Biosciences), anti-CD8a clone 53-6.7 (eBioscience), anti-MHCII (I-A/I-E) clone M5/114.15.2 (eBioscience). Samples were acquired on a Propel Labs YETI / Bio-Rad ZE5 and analysed using FlowJo.

Analysis of platelets

Whole mouse blood was collected into microcentrifuge tubes containing 100 μ l HEPES medium (132mM NaCl, 6mM KCl, 1mM MgSO₄, 20mM HEPES, and 5mM glucose) as previously described². Samples were diluted 2 \times in HEPES medium, and then centrifuged at RT for 15 min at 100 \times g. Platelet rich plasma was incubated for 15 min at RT in 100 μ l of HEPES medium containing the following antibodies: Anti-CD45.2, anti-CD31, anti-CD9, anti-GARP and anti-Ter119 (eBioscience) prior to flow cytometry analysis. Data were acquired using BD Fortessa flow cytometers and analysed using FlowJo (TreeStar).

Cell culture stimulation assays

Total CD4 $^{+}$ T cells were isolated from single-cell spleen suspensions using magnetic negative selection (eBioscience). Cells were stimulated at 37 °C, 5% CO₂ for 16 h in RPMI culture media supplemented with 10% fetal calf serum (Sigma), 1% penicillin and streptomycin (pen/strep; Gibco), and 50 μ M β -mercaptoethanol, non-essential amino acids (Gibco) and Glutamax (Gibco). Cells were plated at density of 1 \times 10⁵ cells/well on 96-well plates in the presence or absence of 10ng/mL recombinant human IL-2 (Peprotech) with or without 300nM Tofacitinib (Sigma) or 10 μ M BI 605906 (Tocris). Where indicated, plates

were coated overnight with 5 µg/mL anti-CD3 (clone 145.2C11; BioXcell Cat #BE0001-1) and 5 µg/mL anti-CD28 (clone 37.51 BioXcell Cat #BE0015-1) monoclonal antibodies in PBS before washing and plating of cells for stimulation. Cells were harvested and analysed by flow cytometry. To detect LPS-induced GARP expression on B cells, cells from erythrocyte-lysed blood were stimulated in RPMI complete media (RPMI, 10% FCS, 1% pen/strep, and 50µM β-mercaptoethanol) containing 0.5 mg/ml lipopolysaccharide (Sigma) at 37 °C, 5% CO₂ for 48 hr. At the end of the stimulation period, cells were collected and analysed using flow cytometry.

Colitis experiments

Average initial body weights prior to induction of colitis were calculated from daily body weight measurements over a period of 1-2 weeks prior to induction of colitis. Colitis experiments were performed in a specialised room within our animal facility with enriched microflora. For dextran sulfate sodium (DSS) colitis experiments, mice were treated with 2% (w/v) DSS (Sigma Aldrich Cat# 42867-100g; Lot #BCBW8358 and #BCCB5021) in the drinking water for up to 16 days. Body weight, general appearance, occult/gross blood loss, and stool consistency were monitored daily to provide an objective clinical severity score. Animals were culled if they had >20% body weight loss or reached a level of clinical severity requiring euthanasia. For analysis of colon length, serum cytokines and gut histopathology, animals were euthanised at 16 days following the initiation of DSS administration and the large intestine was collected. The length of isolated large intestines was measured in a blinded fashion and stored in 10% formaldehyde (Sigma) for subsequent histopathology analysis using haematoxylin and eosin (H&E) staining. Serum samples were also collected from each animal for bead array analysis of serum cytokines. For analysis of cytokine production by T_{conv}, animals were euthanised at 13 days following the initiation of DSS administration and the mediastinal lymph node (mLN) and large intestine were collected. Cytokine expression was measured by flow cytometry after a 4 hour period of restimulation with PMA, ionomycin and BFA.

The T cell transfer colitis model has been described previously³. Briefly, *Rag2*^{-/-} mice were injected intravenously with 4×10^5 FACS-sorted naive CD4⁺ CD25⁻ CD45RB^{high} cells from wildtype (WT) mice with or without 1×10^5 WT or Enh-KO CD4⁺ CD25^{high} T_{reg} cells. Animals were monitored daily for body weight and clinical signs of colitis from which objective clinical severity scores were assigned (Body weight [0-4], general appearance [0-4], occult/gross blood loss [0-4], and stool consistency [0-4]). Colitis-free survival was calculated by measuring the time following cell transfer until the onset of clinical colitis. Events were determined on the basis of severity (combined objective score = 5 on a given day) or chronicity (total combined score = 48 over the preceding 25 days). Animals were censored if they survived to study end without experiencing a colitis event or if the animal was euthanised for severe non-colitis pathology. Animals were culled if they reached 20% body weight loss or a level of clinical severity requiring euthanasia. Sections of large intestine were fixed in buffered 10% formalin and stained with hematoxylin and eosin (H&E).

Isolation and analysis of large intestinal lamina propria lymphocytes

Lamina propria leukocytes (LPL) were isolated from the large intestine (caecum and colon) using the following method: the tissue was removed, washed and cut into 5mm long pieces followed by incubating at room temperature in 10mL PBS containing 1 μ L of 1M DTT for 10 minutes with gentle shaking. The samples were filtered through 70 μ m cell strainers with 10mL RPMI-2 (RPMI supplemented with 1% HEPES and 2% FCS). The remaining tissues on the strainer were digested twice in 10mL RPMI-2 with 30mM EDTA at 230 rpm, 37 °C for 10 minutes and the filtrate discarded. The remaining tissues were homogenised into small pieces and digested in 6 mL of RPMI-2 containing 0.05 mg/mL collagenase VIII (Sigma) and 0.15 mg/mL DNase I (Roche) at 37 °C for 45 minutes with gentle shaking. The sample was then filtered for density gradient as the LPL sample. Isolated LPL was resuspended in 6mL 40% Percoll (Sigma) and underlaid with 1mL 80% Percoll for centrifugation. Centrifugation was carried out without brake at 2300 rpm for 25 minutes at room temperature. The interface was extracted, pelleted and resuspended in RPMI-2 for subsequent analysis by flow cytometry.

RNA-Seq analysis

CD4 $^{+}$ *Foxp3* $^{GFP+}$ T_{reg} and CD4 $^{+}$ *Foxp3* $^{GFP-}$ T_{conv} cells were sorted by FACS from WT and Enh-KO *Foxp3* GFP reporter animals. Briefly, total CD4 $^{+}$ T cells were pre-enriched from single cell spleen suspensions using magnetic negative selection (eBioscience) prior to FACS-sorting of GFP $^{+}$ and GFP $^{-}$ CD4 $^{+}$ T cells using a BD Influx instrument (Becton Dickinson Biosciences). Cells were sorted into solutions of RPMI 1640 medium supplemented with 20% FBS and pellets were stored in RNAlater (Ambion) at -80°C. Total RNA was extracted using the RNeasy Plus Mini Kit (Qiagen) according to manufacturer instructions. Barcoded libraries were prepared using the SmartSeq2 protocol as previously described⁴ using a Hamilton NGS-STAR library preparation automation system at the BI Sequencing Facility and sequenced using a HiSeq 2500 (Illumina).

RNA-seq reads were trimmed using Trim Galore v0.4.4 using default parameters to remove the Nextera adapter sequence. Mapping was performed using HISAT2 v2.1.0 against the mouse NCBIM37 genome, guided by gene models from Ensembl annotation release 68. Aligned fragments were imported into SeqMonk (v1.44.0) and filtered to remove mappings with MAPQ scores of <20. Differential gene expression analysis was performed using the DESeq2 algorithm within SeqMonk.

Analysis of STAT5 binding

Naïve CD4 $^{+}$ CD62L $^{+}$ CD44 $^{-}$ cells were sorted by FACS and stimulated on anti-CD3-coated plates in the presence of recombinant human IL-2 (5g/ml), TGF- β (2ng/mL) and anti-CD28 (2 μ g/mL) for 4 days. Cells were washed thrice in complete media and rested overnight in complete medium without IL-2. The following day, cells were stimulated with or without 50ng/ml IL-2 for 1 hour and immediately chemically cross-linked using methanol-free formaldehyde (1% final w/v) at 37 °C for 10 minutes and the reaction was quenched with glycine. 1 \times 10⁷ cells per ChIP replicate were sonicated to generate fragmented chromatin which was subjected to immunoprecipitation using anti-STAT5B (R&D AF1584) to detect STAT5 binding. For PCR-based confirmation of STAT5 binding, qPCR reactions were

carried out on input and immunoprecipitated DNA using the Power SYBR Green kit (Applied Biosystems) and the following primers: Lrrc32+70k_FW1, GAGCTGG GTGGTGG ATAACA; Lrrc32+70k_RV1, CCAAGAAAA GGCGGTGTTT; Foxp3_CNS2_FW1, ATCTGGCCA AGTCAGGT TGTGAC; Foxp3_CNS2_RV1, GGGCGTTCC TGTTTGACT GTTTCT; Lrrc32_pro_FW1, CCTTCTCCCT CCAGTCGTTT; Lrrc32_pro_RV1, CGCCCCCTT TTAAATAGC.

Analysis of genome-wide chromatin accessibility using ATAC-Seq

Genome-wide measurement of chromatin accessibility and computational alignment of generated data were performed from biological replicates using ATAC-Seq on FACS-sorted CD4⁺ *Foxp3*^{GFP+} T_{reg} and CD4⁺ *Foxp3*^{GFP-} T_{conv} cells from *Foxp3*^{GFP} reporter animals as previously described⁵. ATAC-seq reads were trimmed using Trim Galore (v0.4.4) using default parameters to remove standard Illumina adapter sequences. Reads were mapped to the mouse NCBIM37 genome assembly using Bowtie2 v2.3.2 with default parameters. TDF files for analysis in the IGV genome browser were generated using Samtools v1.9 and Igvtools v2.3.26 and differential accessibility of called peaks (MACS) was assessed using Diffbind.

Analysis of serum cytokines

Blood was collected into microcentrifuge tubes without anti-coagulants and centrifuged at 400 × g for 5 min. Supernatants were collected into fresh tubes and centrifuged at 16,000 × g for 10 min and stored at -80 °C until further analysis. Serum was analysed using the MesoScale Discovery Mouse proinflammatory cytokine bead array (MSD; K15048D-2) at the Core Biochemical Assay Laboratory at the University of Cambridge.

Syntenic alignment

Synteny data and alignment blocks were obtained from human:mouse LASTz alignments extracted from Ensembl compara database v90. Chromosomal synteny was also taken from compara and LASTz pairwise alignments. The search is run in two steps; first, we searched for alignment blocks that were in the same order in the two genomes. Syntenic alignments that were closer than 200Kb were grouped into a synteny block; second, groups that were in synteny were linked, provided that no more than two non-syntenic groups were found between them and they were less than 3Mb apart. For analysis of evolutionarily conserved TF binding sites, we used the phyloP evolutionary conservation analysis providing basewise conservation among 30 placental mammals (phyloP30wayPlacental) to determine the level of evolutionary conservation at specified regulatory elements within the enhancer⁶. Evolutionarily conserved predicted TF binding motifs were identified using ECR Browser (<https://ecrbrowser.dcode.org/>)

Human T_{reg} cell hQTL and eQTL analysis

Leukocyte cones were obtained with informed consent with Research Ethics Committee (REC) approval from donors at NHS Blood and Transplant, Cambridge (REC 15/NW/0282) and from the NHS Blood and Transplant, Oxford (REC 15/NS/0060) and experiments involving human samples complied with all relevant ethical regulations. T_{reg}s from 135

Europe PMC Funders Author Manuscripts

Europe PMC Funders Author Manuscripts

healthy adults of Caucasian origin were obtained from leukodepletion cones. PBMCs were isolated using Lympholyte-H (Cedrelane Labs, Burlington, Canada) density gradient centrifugation. CD4⁺ T cells fraction of the PBMCs was obtained by negative selection using EasySep® Human CD4+ T Cell Enrichment Kit (Cat. no. 19052, StemCell Technologies, Vancouver, Canada), following the manufacturer's instructions. CD4⁺ CD127⁻ CD25⁺ T_{reg} cells were isolated by FACS. Genomic DNA was extracted from each sample and subjected to genotyping using the Infinium® CoreExome-24 v1.1 BeadChip (Illumina). The genotyping data were imputed using the 1000 Genomes Phase 3 reference panel and BEAGLE 4.17⁷. T_{reg} cells obtained from each individual underwent RNA-seq (123 individuals) or genome-wide measurement of H3K27ac using ChIPmentation-seq (91 individuals)⁸. A total of 1.86 million read pairs were downsampled from each donor per H3K27ac ChIPmentation-seq assay and merged. Then, H3K27ac broad peaks were called using MACS2⁹ and only peaks with fold enrichment ≥ 2 and adjusted p-value < 0.001 were maintained in the final set. Gene and peak read counts were obtained using featureCounts¹⁰. Quantitative trait loci (QTL) for gene expression and H3K27ac were evaluated using linear models with QTLtools¹¹. Principal components that explained up to 1% of the observed variance per assay were included as covariates. Colocalization between QTLs and immune disease GWAS loci was performed using coloc v2.3¹² and using a 400-kb window around each lead QTL variant located within 100kb from each GWAS variant (nominal p value $< 10^{-5}$), as described¹³.

For eQTL analysis of signal-driven GARP expression on T_{reg} cells, PBMC were collected from presumed healthy donors at the Policlinico San Matteo Pavia Fondazione IRCCS and 1×10^7 cells per donor were cryopreserved for later analysis. Following cryorecovery, cells were stimulated at 37 °C, 5% CO₂ for 16 h in RPMI culture media supplemented with 10% fetal calf serum (Sigma), 1% penicillin and streptomycin (pen/strep; Gibco), and 50µM β-mercaptoethanol, non-essential amino acids (Gibco) and Glutamax (Gibco). Cells were plated at a density of 1×10^6 cells/well on 24 well plates in the presence or absence of 50ng/mL recombinant human IL-2 (Peprotech) and plate-bound anti-CD3 (0.2µg/mL; clone OKT3 BioXcell Cat# BE0001-2) and anti-CD28 (0.2µg/mL; clone 9.3 BioXcell Cat# BE0248) monoclonal antibodies. For genotyping of individuals, cells were harvested and analysed by flow cytometry. Genomic DNA extracted from PBMC were subjected to PCR-based amplification using the following primers: Fw1: 5'-AAAGCATGGCTGAGAAAACC-3' and Rv1: 5'-CCAGGGAGGAAGTTCTGGAG-3' yielding an amplicon containing rs11236797 and forward and reverse Sanger sequencing reactions were primed using Fw1 and Rv2 (5'-ACAGTGCTGACTGAGAGGAA-3', respectively.

HiChIP virtual 4C (v4C) analysis

v4C analyses were performed using matrices generated by Juicebox. The Juicebox tools *dump* command was used to extract the chromosome of interest from the .hic file¹⁴. The interaction profile of the specific 5 kb bins containing the promoter and enhancer anchors were then plotted in R. Replicate reproducibility was visualized with the mean profile shown as a line and the shading surrounding the mean representing the standard deviation between

replicates. The *p* value was calculated using Student's *t* test comparing the replicate read support for the promoter to enhancer interaction in Treg cells versus naïve T cells.

Lentiviral plasmid construction and virus production

Lenti sgRNA(MS2)_zeo (plasmid 61427; Addgene), dCas9-VP64_GFP (plasmid 61422; Addgene) and Lenti MS2-P65-HSF1_Hygro (plasmid 61426; Addgene)¹⁵ vectors were gifts from F. Zhang. DNA sequences of single guide RNAs (sgRNAs) for CRISPR activation were designed using Custom Alt-R® CRISPR-Cas9 guide RNA design tool (https://www.idtdna.com/site/order/designtool/index/CRISPR_CUSTOM) and are listed in Supplementary Table 6. All sequences were selected to precede a NGG protospacer-adjacent motif sequence. Cloning of sgRNAs into Lenti sgRNA(MS2)_zeo was performed as previously described¹⁶. For the production of Lentiviruses pseudotyped with the vesicular stomatitis virus G protein envelope, plasmid DNA was co-transfected with vesicular stomatitis virus G protein, pLP1, and pLP2 plasmids into HEK293T cells (ATCC; mycoplasma-free low passage stock) using Lipofectamine 3000 (Invitrogen) according to the manufacturer's protocol and as previously described¹⁶.

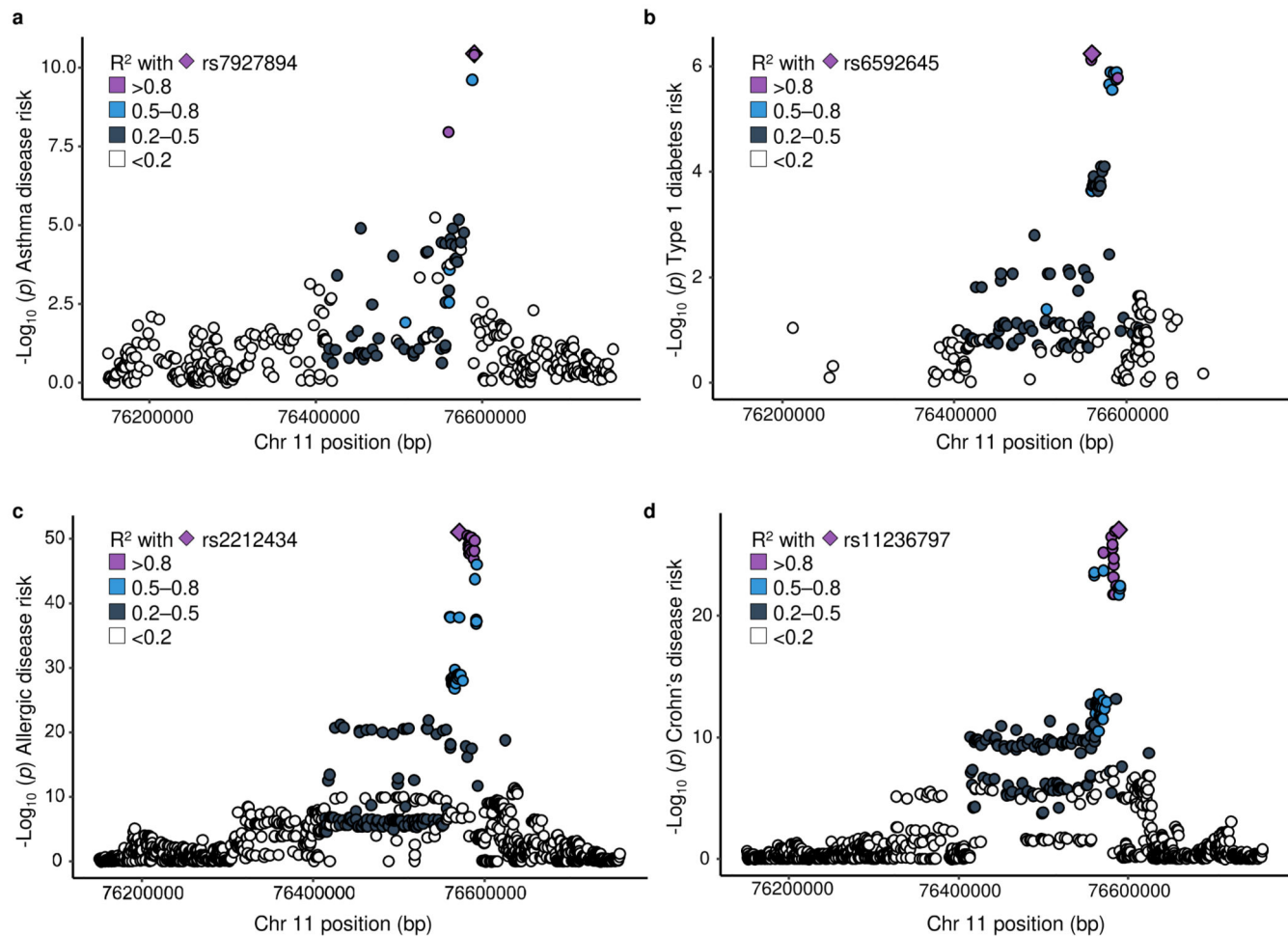
PBMCs were obtained with from healthy individuals at New York Blood Center (NYBC), New York, NY with NYBC Institutional Review Board (IRB) approval and experiments complied with all relevant ethical regulations. Lymphocytes were isolated using Ficoll-Paque plus (GE Healthcare). CD4⁺ T cells were isolated using Dynal CD4⁺ isolation kits (Invitrogen). Purified CD4⁺ T cells were stimulated using anti-CD3/anti-CD28 Dynabeads (Invitrogen) and cultured in complete RPMI 1640 medium (RPMI 1640 supplemented with 10% FBS; Atlanta Biologicals, Lawrenceville, GA) containing IL-2 (10 ng/ml) as described¹⁶. One day after activation, cells were transduced with dCas9-VP64_GFP and Lenti_MS2-P65-HSF1_Hygro lentiviral vectors at MOI of 5-10. Cells were then selected with 250 µg/ml hygromycin 3-5 days post-infection and expanded for 2 weeks. Antibiotic selection was performed for 3–5 days or until 95% of non-transduced cells were dead. Expanded and hygromycin-selected T cells expressing dCas9-VP64_GFP and P65 were then re-stimulated with anti-CD3/anti-CD28 beads and transduced with lentiviruses encoding Enhancer-targeting sgRNAs in Lenti-sgRNA_(MS2) at a MOI of 5-10. Cells were harvested 5 days after transduction and analysed by flow cytometry on a SP6800 spectral cell analyser (Sony Biotechnology, CA). Data analysis was performed using FlowJo software (TreeStar Inc, Ashland, OR).

Statistical analysis

Where relevant, sample sizes were determined using power calculations based on variability observed in prior experiments of a similar kind or using prior experience of sample size requirement. For experiments where technical limitations prevented adequate statistical power to be obtained from single experiments, results from multiple experiments were pooled to provide sufficient statistical power. Pre-established exclusion criteria across samples from a given experiment were used to avoid subjective bias. Experiments included positive and negative controls to allow technical failure of experiments to be objectively determined. Data reported are in most cases non-subjective and did not require randomisation or blinding at measurement. However, where appropriate, experimental

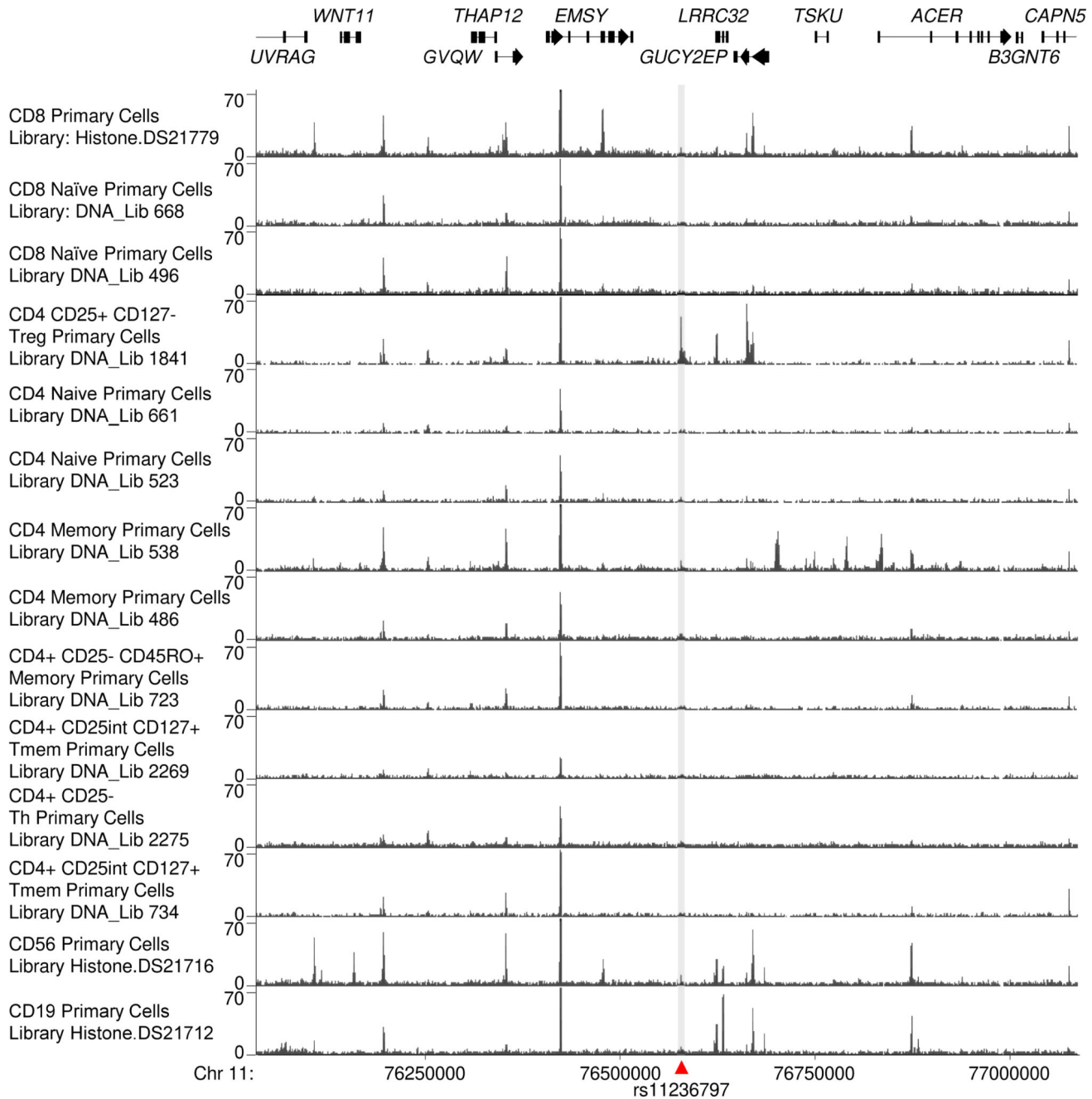
cohorts were composed of randomised age- and sex-matched animals or subject to random Mendelian segregation of genotypes within litters. Investigators were not formally blinded. However, in randomised experiments it was difficult for investigators and technicians to readily determine genotypes from animal IDs at the bench.

Extended Data



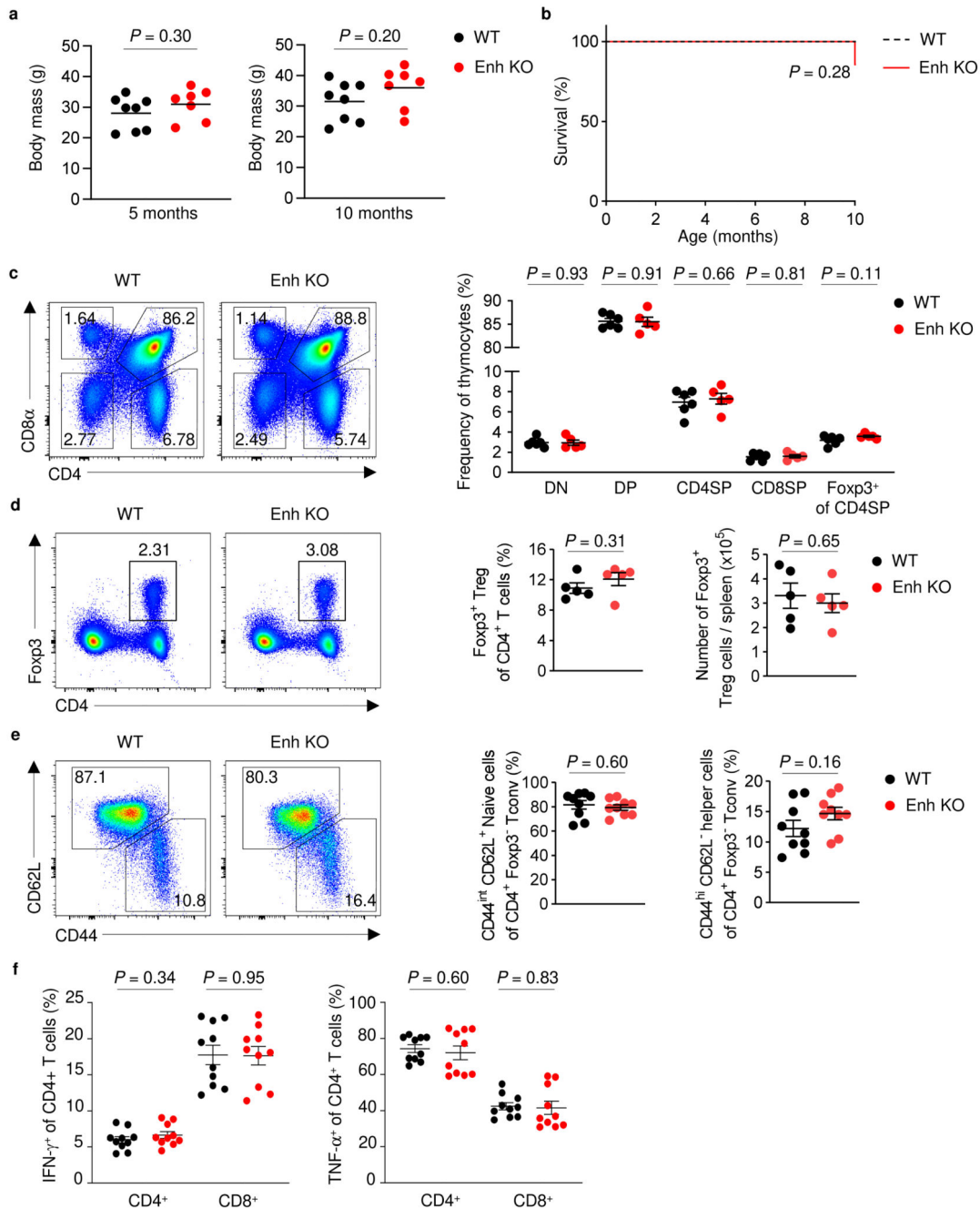
Extended Data 1. Highly linked genetic polymorphisms at a distal intergenic region of 11q13.5 are associated with risk of multiple immune-mediated diseases.

a-d, Graph showing association of polymorphisms within the 11q13.5 locus with risk of indicated immune-mediated disorders (- $\text{Log}_{10}(p)$; left axis). Each point represents an individual single-nucleotide polymorphism (SNP). Point colours depict R^2 values reflecting the level of linkage disequilibrium between each polymorphism and the indicated lead GWAS variant (diamond symbol). Chromosomal position (GRCh38) is represented on the x-axis. GWAS summary statistics and replicate information from Demenais *et al.* (a), Onengut-Gumuscu *et al.* (b) Ferreira *et al.* (c) and de Lange *et al.* (d)^{2,4,6}.



Extended Data 2. Alignments showing distribution of H3K27Ac at the indicated genomic region in primary human lymphocytes.

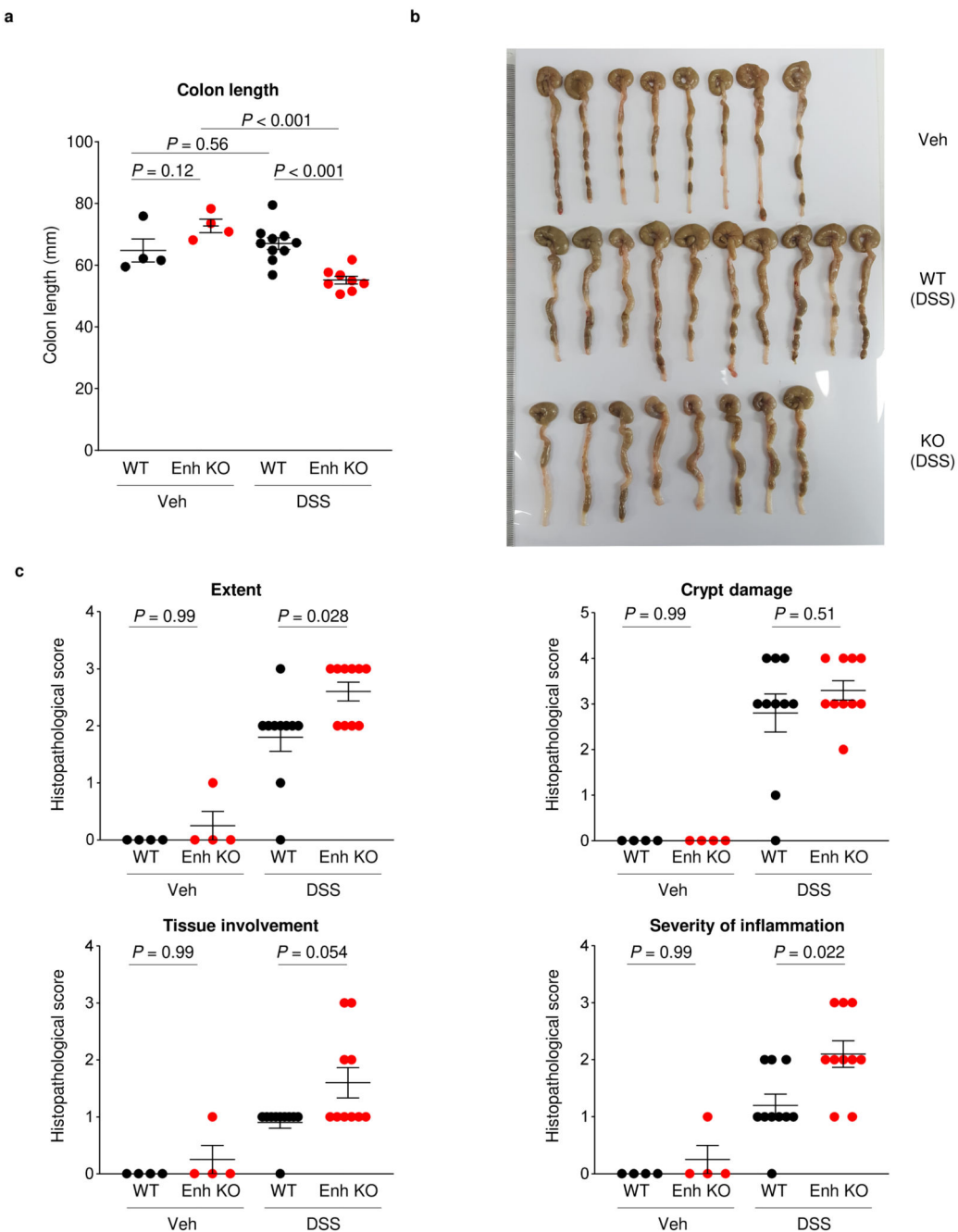
Alignment of H3K27Ac enrichment at the indicated locus within the indicated lymphocyte lineages; Roadmap Epigenomics Project for sample information and replicate statistics⁸. Grey shaded area marks the risk locus containing the single nucleotide polymorphism (SNP) rs11236797 (position indicated by red triangle).



Extended Data 3. Steady-state immune phenotype of Enh-KO animals.

a-b, Body mass at indicated age (**a**) and Kaplan-Meier plot showing survival (**b**) of animals of indicated genotypes (n=8 and 7, WT and Enh-KO from 8 independent breedings). **c**, Representative flow cytometry (left) and replicate measurements (right) of the frequency of the indicated thymocyte subsets in the thymi of animals of the indicated genotypes at 8–10 weeks of age (n=6 and 5; WT and Enh-KO). **d**, Representative flow cytometry (left) and replicate measurements of the frequency and absolute number (right) of Foxp3⁺ T_{reg} cells in the spleens of animals of the indicated genotypes at 8–10 weeks of age (n=5 mice per group).

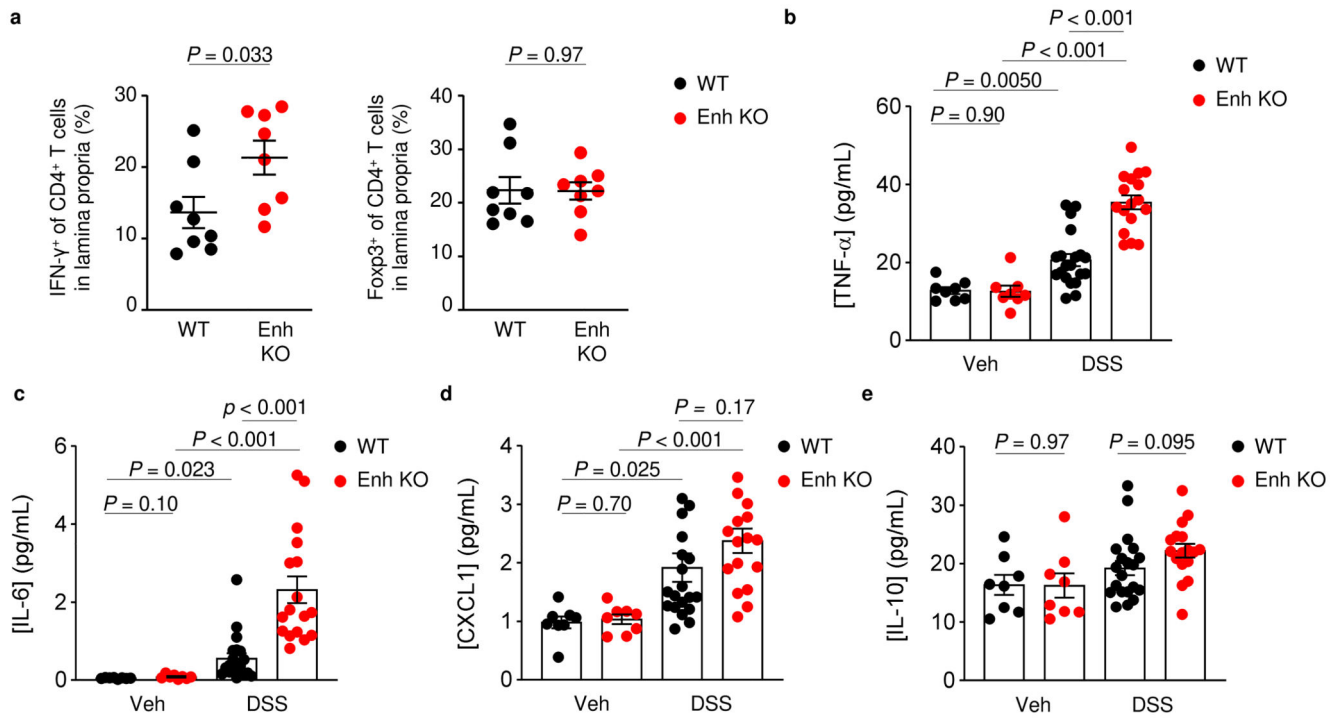
Representative of 2 independent experiments (**c-d**). **e**, Representative flow cytometry (left) and replicate measurements of the frequency of naïve and helper CD4⁺ Foxp3⁻ T_{conv} cells in the spleens of animals of the indicated genotypes at 8-10 weeks of age (n=9 mice per group, pooled from two independent experiments). **f**, Frequency of cells expressing IFN- γ (left) and TNF- α (right) upon intracellular cytokine staining analysis of splenic CD4⁺ and CD8⁺ T cells from animals of the indicated genotypes at 8-10 weeks of age (n=10 mice per group pooled from two independent experiments). Unpaired two-tailed Student's *t* test (**a, c-f**), Mantel-Cox test (**b**). Bars and error show mean and s.e.m.



Extended Data 4. Increased susceptibility of Enh-KO animals to DSS colitis induced by dextran sulphate sodium (DSS).

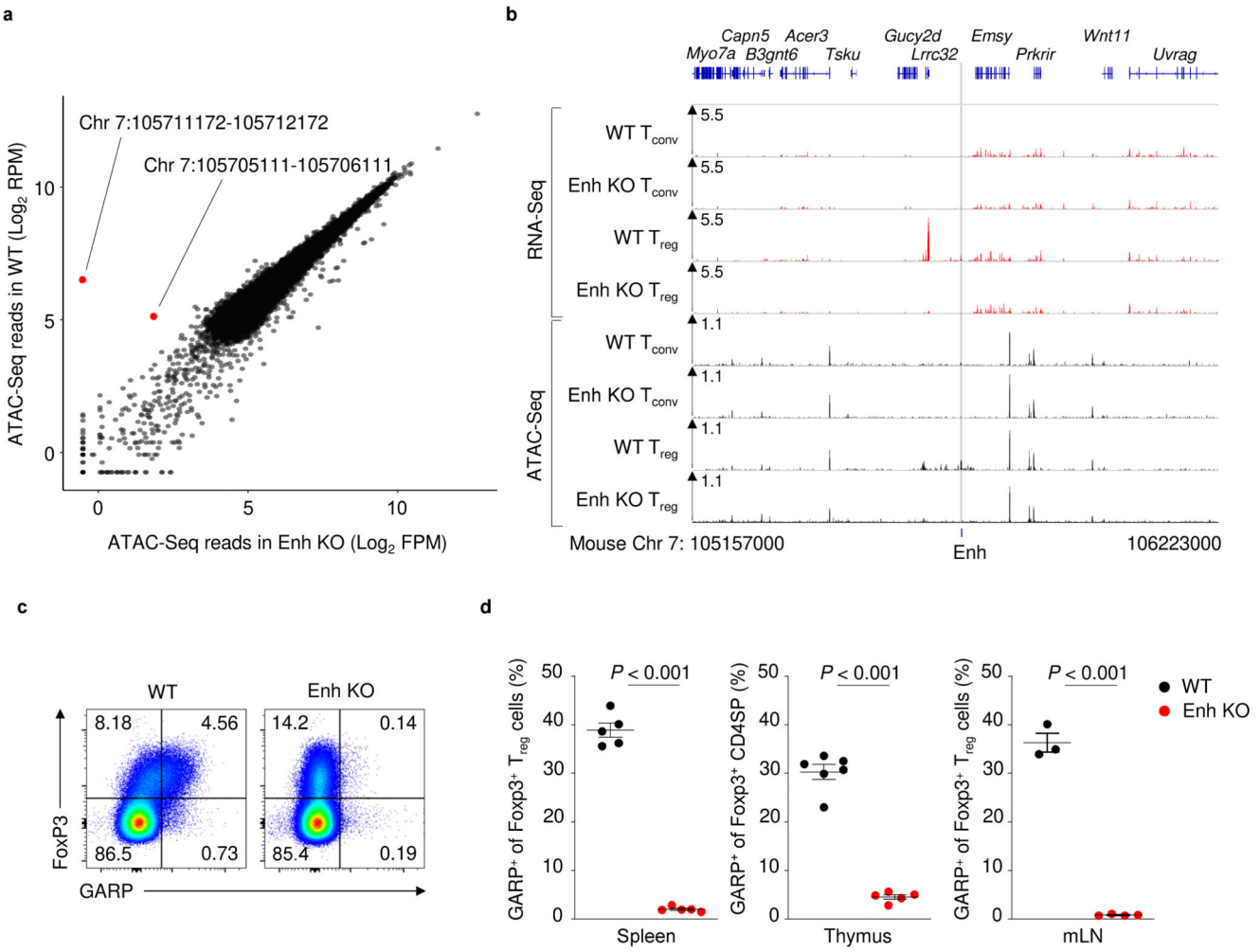
a-b, Replicate length measurements (**a**) and photographs (**b**) of large intestine from WT and Enh-KO mice treated with DSS or vehicle control (Veh). n=4, 4, 10 and 8; WT (Veh), Enh-KO (Veh), WT (DSS), Enh-KO (DSS). **c,** Histopathological scores of sections of large intestine from WT and Enh-KO treated for 16 days with DSS or Veh. The following scoring criteria were used: Extent of inflammation: 0, none; 1, mucosa; 2, mucosa & submucosa; 3, transmural. Crypt damage: 0, none; 1, basal one-thirds; 2, basal two-thirds; 3, only surface

epithelium intact; 4, loss of entire crypt and surface epithelium. Tissue involvement: 1, 0 to 25%; 2, 26 to 50%; 3, 51 to 75%; 4, 76 to 100%. Severity of inflammation: 0, none; 1, mild; 2, moderate; 3, severe. Data are representative of two independently repeated experiments with 10 and 4 mice per DSS- and Veh-treated group. Unpaired two-tailed Student's *t* test (**a**); Wilcoxon-Mann-Whitney Test (**c**). Bars and error show mean and s.e.m.



Extended Data 5. Analysis of cytokine expression in WT and Enh-KO animals treated with DSS.

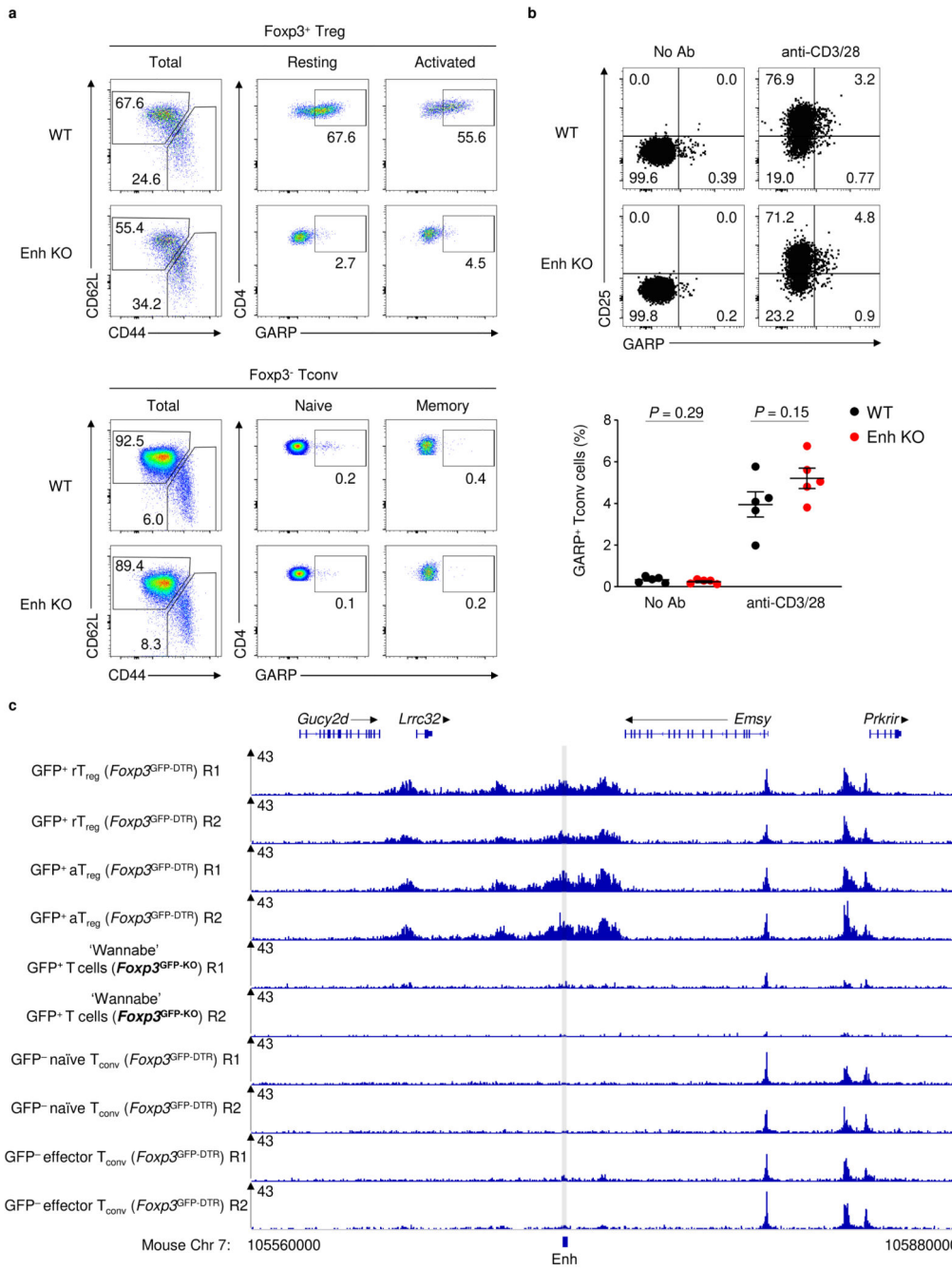
a, Replicate measurements of IFN- γ (left) and Foxp3 (right) by large intestinal lamina propria CD4⁺ T cells (n=8 mice per group). Data representative of two independent experiments. **b-e**, Concentration of the indicated cytokines in the serum of WT and Enh-KO animals treated with Veh or DSS for 16 days. Data pooled from two independent experiments with n=8, 8, 20 and 17 for WT (Veh), Enh-KO (Veh), WT (DSS), Enh-KO (DSS) groups. Data analysed using unpaired two-tailed Student's *t* test. Bars and error show mean and s.e.m.



Extended Data 6. Loss of *LRRC32* / GARP expression on Foxp3⁺ T_{reg} cells from Enh-KO animals.

a, Scatterplot showing global differences in chromatin accessibility at called peaks using ATAC-Seq analysis of WT and Enh-KO CD4⁺ *Foxp3*^{EGFP} T_{reg} cells. Red dots show significantly differentially accessible peaks (FDR<0.05). Mean Log2 reads per million (RPM) values for each called peak (represented as points) from 3 independent biological replicates are shown, with samples isolated on different days. Two-tailed Wald test with Benjamini-Hochberg correction. **b**, Representative alignment of gene expression (top) and chromatin accessibility (bottom) within the indicated cell types sorted by FACS from WT and Enh-KO *Foxp3*^{EGFP} reporter animals. Expected loss of ATAC-Seq reads mapping to the deleted region (Enh; highlighted in grey) in Enh-KO cells is observed. Data representative of three independent biological replicates with samples isolated on different days. **c**, Representative flow cytometry analysis of GARP and Foxp3 expression by CD4⁺ T cells of animals of the indicated genotypes from mLN. **d**, GARP expression from animals of indicated genotypes in spleen (n=5 per genotype), thymus (n=6 and 5 for WT and Enh-KO groups), and mLN (n=3 and 4 for WT and Enh-KO groups). Data are representative of 3 and

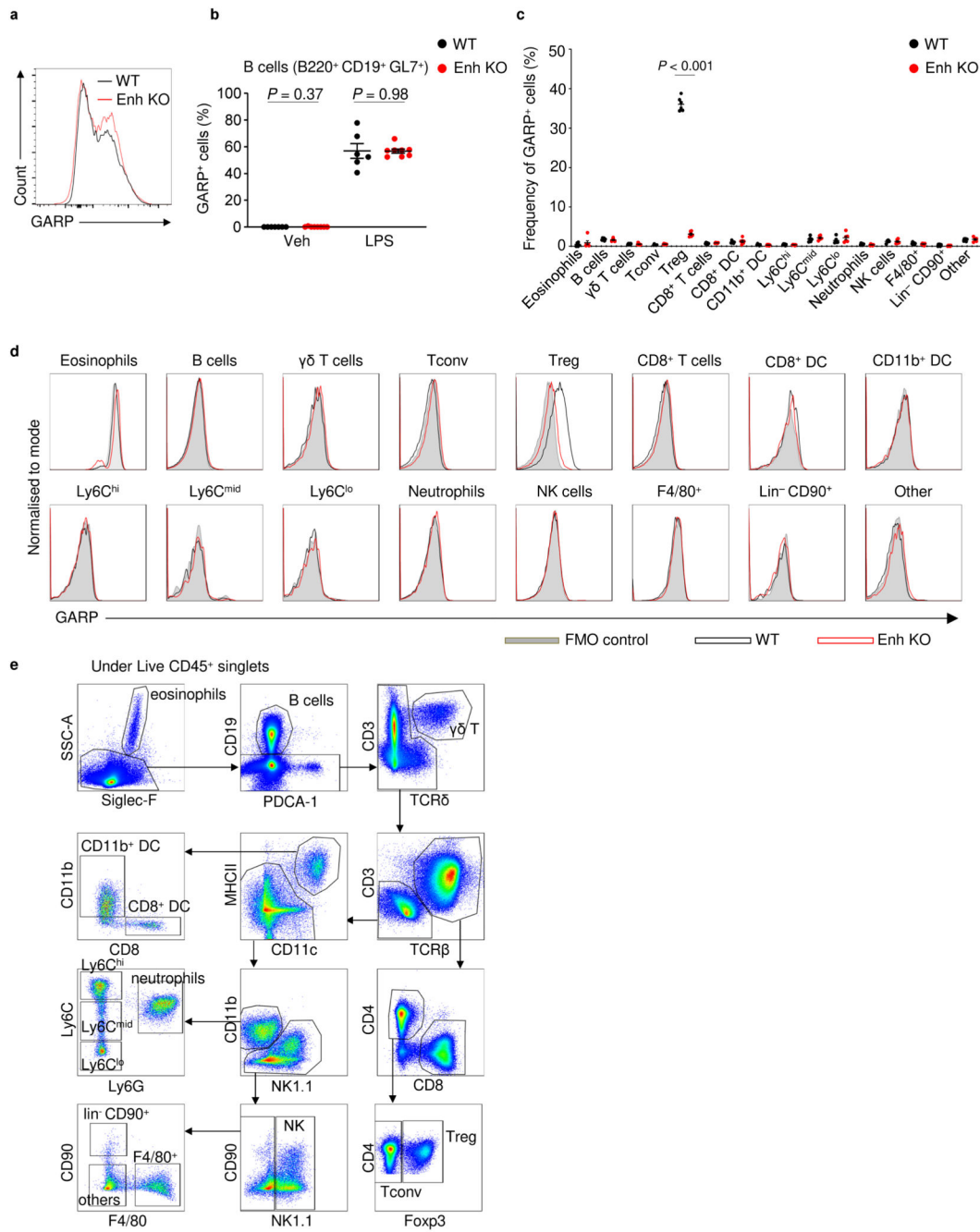
2 independent experiments (**c-d**). Unpaired two-tailed Student's *t* test (**d**). Bars and error show mean and s.e.m.



Extended Data 7. *Lrrc32* +70k is not required for induction of GARP on the surface of CD4⁺ T_{conv} cells following stimulation *in vitro*.

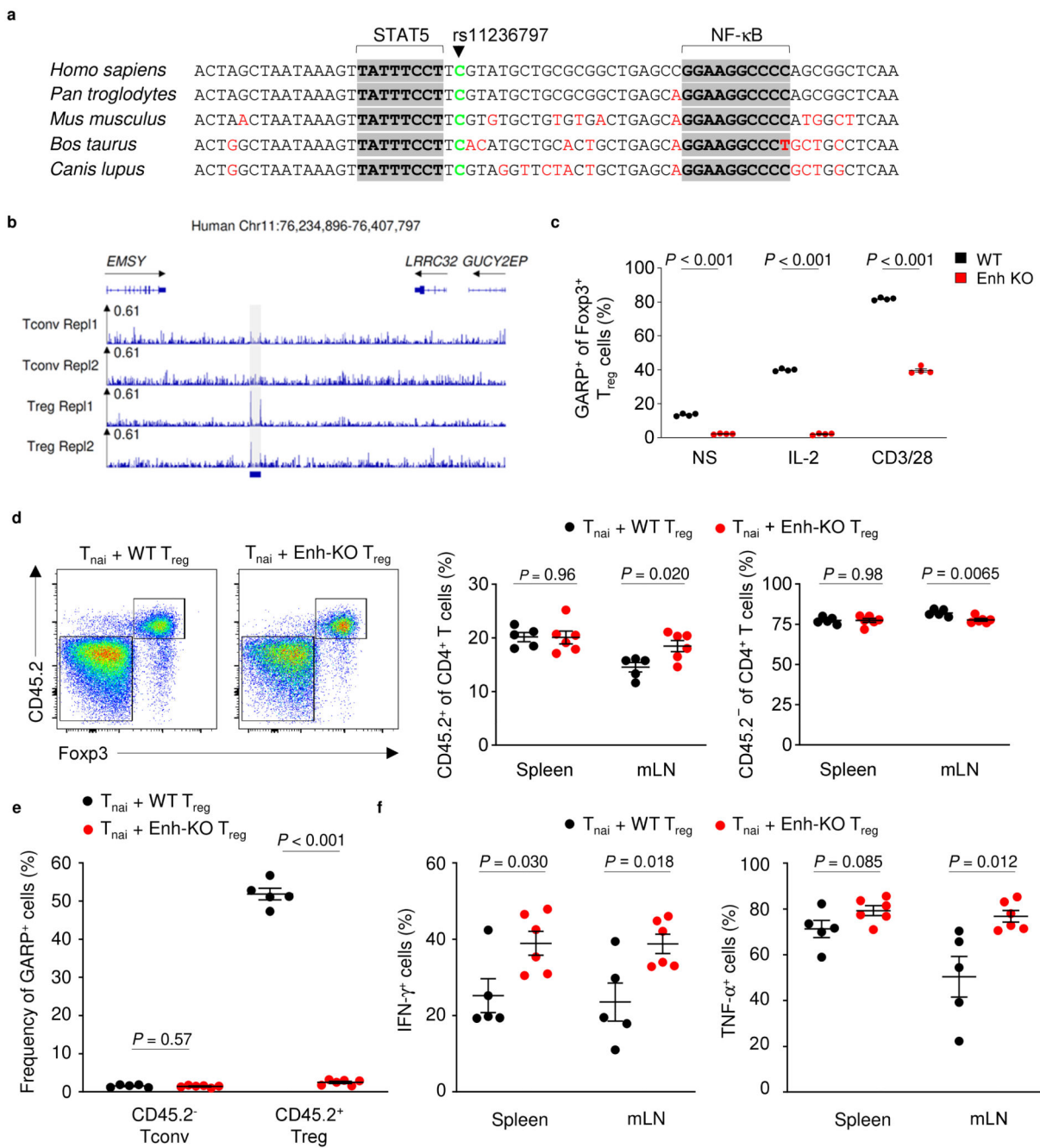
a, Representative flow cytometry showing gating strategy and representative GARP expression on resting (CD44^{lo} CD62L⁺) and activated (CD44^{hi} CD62L⁻) T_{reg} cells (top) and naïve (CD44^{lo} CD62L⁺) and memory (CD44^{hi} CD62L⁻) T_{conv} cells (bottom). Data are representative of two independent experiments. **b**, Representative flow cytometry (top) and

replicate measurements (bottom) of CD25 and GARP expression on CD4⁺ Foxp3⁻ T_{conv} cells following stimulation under the indicated conditions for 16 h *in vitro*. Data representative of 3 independently repeated experiments with 5 independent biological replicates per group. **c**, Representative alignments of known H3K27Ac ChIP-Seq data from the indicated cell types. Arvey *et al.* for sample information and replicate statistics²⁰. Grey bar shows position of the enhancer. Unpaired two-tailed Student's *t* test (**b**). Bars and error show mean and s.e.m.



Extended Data 8. Specific loss of GARP expression on T_{reg} cells from Enh-KO animals.

a, Representative flow cytometry of GARP expression on CD45⁻ CD31⁺ endothelial cells from lungs of WT and Enh-KO animals. **b**, Frequency of GARP⁺ cells among WT and Enh-KO B220⁺ CD19⁺ GL7⁺ cells, stimulated with bacterial lipopolysaccharide (LPS) or vehicle control (Veh) for 48 h (n=6 and 8 for WT and Enh-KO groups). **c**, Percentage of GARP⁺ cells among indicated cell types from WT and Enh-KO animals (n=6 per genotype; unpaired two-tailed Student's *t* test). **d**, Representative histograms showing GARP expression in the cell types shown in **c**. **e**, Representative flow cytometry indicating gating strategy for cells shown in **c**. Unpaired two-tailed Student's *t* test (**b**). Data are representative of two independent experiments. Bars and error show mean and s.e.m.

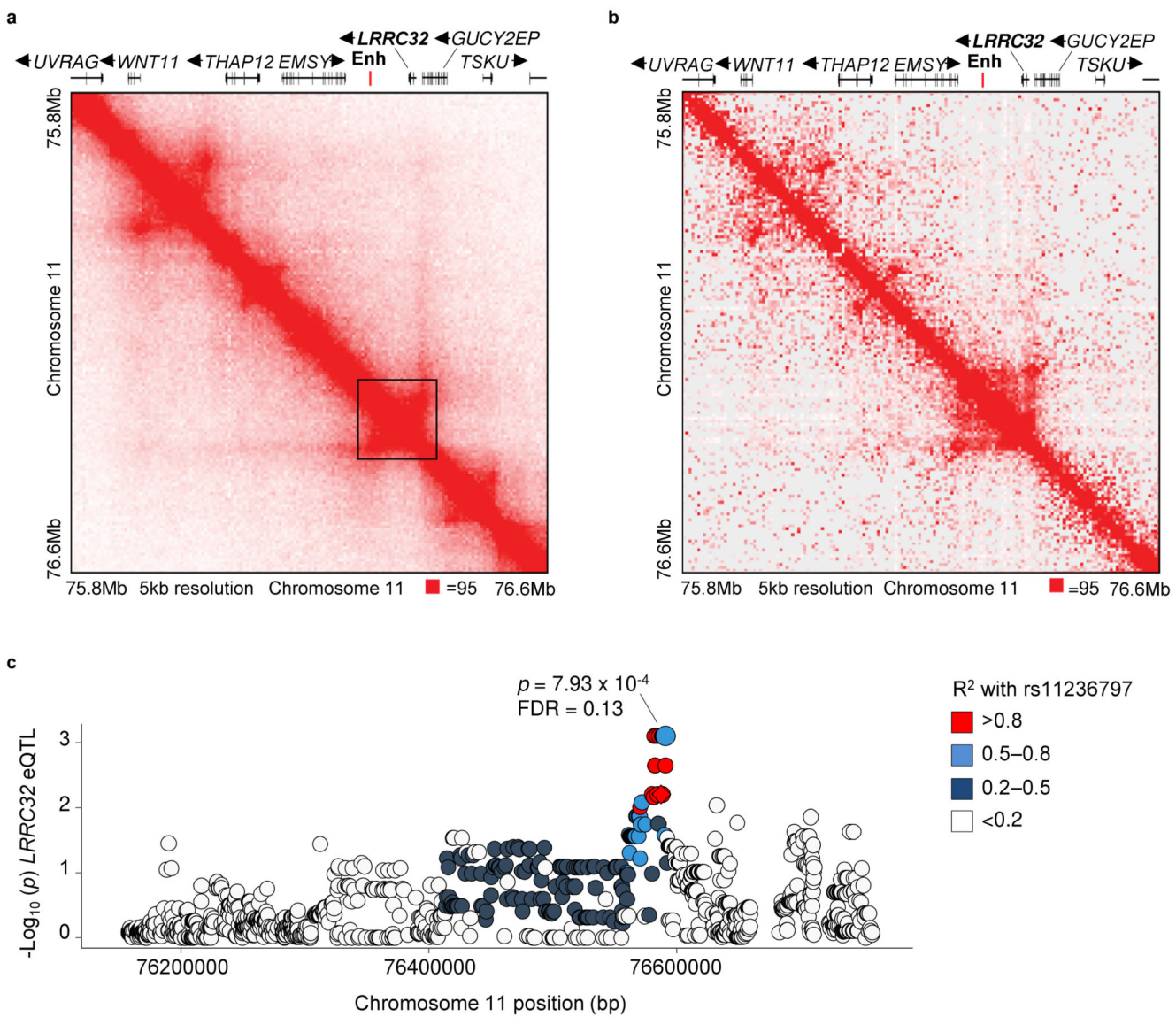


Extended Data 9. Molecular and functional characterisation of mouse and human enhancer homologs.

a, Evolutionarily conserved STAT5 and NF-κB binding motifs within *Lrrc32*+70k.

Genomic sequence alignments of reference genome sequences of indicated mammals are shown. The position of conserved STAT5 and NF-κB binding motifs (V\$STAT5A_03 and V\$NFKAPPAB_01, respectively) are highlighted in grey. The position of rs11236797 is shown. **b**, Alignment of previously determined STAT5 ChIP-Seq binding at the indicated locus in human T_{reg} and T_{conv} cells. Schmidl *et al.* for sample information and replicate

statistics²¹. The identified distal enhancer is shown indicated by the grey shaded area. **c**, GARP expression on CD4⁺ Foxp3⁺ T_{reg} cells following stimulation under the indicated conditions for 16 h *in vitro*. n=4 technical replicates per condition; data are representative of 3 independent experiments. **d**, Representative flow cytometry showing gating (left) and replicate measurements (right) of CD45.2⁺ (transferred T_{reg}) and CD45.2⁻ (transferred T_{conv}) cells within the spleen and mLN of cell transfer recipients. **e**, Replicate measurements of GARP expression on the indicated cell types from the spleen. **f**, Replicate measurements of expression of indicated cytokines by CD45.2⁻ T_{conv} cells from indicated tissues following brief restimulation *ex vivo*. n=5 and 6, WT and Enh-KO T_{reg} recipients (**d-f**). Data representative of two independent experiments. Unpaired two-tailed Student's *t* test (**c-f**). Bars and error show mean and s.e.m.



Extended Data 10. Conformational topography and eQTL analysis of human 11q13.5.

a, Visualisation of intrachromosomal interactions at human 11q13.5 within the B lymphoid line GM12878²⁹. A sub-topologically associated domain containing the identified enhancer and the promoter of *LRRC32* is indicated. Rao *et al.* for sample information and replicate statistics²⁹. **b**, Analysis of intrachromosomal H3K27Ac-enriched HiChIP interactions within human CD4+ naïve (CD45RA⁺ CD25⁻ CD127^{hi}), T_{reg} (CD25⁺ CD127^{lo}), and T helper (Th)17 cells (CD45RA⁻ CD25⁻ CD127^{hi} CCR6⁺ CXCR5⁻) isolated directly from human peripheral blood. Mumbach *et al.* for sample information and replicate statistics²⁸. **c**, Expression quantitative trait locus (eQTL) analysis of the association between genetic polymorphisms at the indicated SNP with *LRRC32* expression in human CD4⁺ CD127⁻ CD25⁺ T_{reg} cells isolated by FACS from the blood of 123 healthy human donors. Point colours reflect linkage disequilibrium (R^2) relative to rs11236797. Nominal *p* value and false discovery rate (FDR) of the most significantly associated SNP are shown; linear regression, two-sided.

Supplementary Material

Refer to Web version on PubMed Central for supplementary material.

Acknowledgements

The research was supported by Wellcome Trust / Royal Society Fellowship 105663/Z/14/Z, Wellcome Trust grant WT206194, Biotechnology and Biological Sciences Research Council grants BB/N007794/1, BBS/E/B/000C0427 and BBS/E/B/000C0428, Cancer Research UK grant C52623/A22597, MRC grants MR/N014995/1, MR/S024468/1 and MC_UU_00014/5, Wellcome Trust Major Award 208363/Z/17/Z, Associazione Italiana per la Ricerca sul Cancro (AIRC) grant IG 20607, and US National Institutes of Health (NIH) grants RM1-HG007735, U19-AI142733 and R01-AI121920. We thank members of the Babraham Institute Biological Services Unit, flow cytometry facility and sequencing facility, and Wellcome Sanger Institute flow cytometry, sequencing, IT and data access facilities for data generation and processing. We thank all participating blood donors, and Cambridge and Oxford NHS Blood and Transplant, New York Blood Center and Policlinico San Matteo Pavia Fondazione for the recruitment of study participants. We thank Federica De Paoli (Humanitas) for processing human PBMC samples and Martin Turner, Klaus Okkenhaug, Ethan Shevach, Michelle Linterman and Geoff Butcher for support and discussion.

Data Availability

RNA-Seq data are deposited in the Gene Expression Omnibus (GEO) database under the accession number GSE128198. Sequencing data for H3K27Ac hQTL and mRNA eQTL analyses are deposited under the European Genome-phenome Archive (EGA; study accession EGAS00001003516, datasets EGAD00001004828 and EGAD00001004830).

References

1. Maurano MT, et al. Systematic localization of common disease-associated variation in regulatory DNA. *Science*. 2012; 337:1190–1195. DOI: 10.1126/science.1222794 [PubMed: 22955828]
2. de Lange KM, et al. Genome-wide association study implicates immune activation of multiple integrin genes in inflammatory bowel disease. *Nature genetics*. 2017; 49:256–261. DOI: 10.1038/ng.3760 [PubMed: 28067908]
3. Anderson CA, et al. Meta-analysis identifies 29 additional ulcerative colitis risk loci, increasing the number of confirmed associations to 47. *Nature genetics*. 2011; 43:246–252. DOI: 10.1038/ng.764 [PubMed: 21297633]

4. Onengut-Gumuscu S, et al. Fine mapping of type 1 diabetes susceptibility loci and evidence for colocalization of causal variants with lymphoid gene enhancers. *Nat Genet*. 2015; 47:381–386. DOI: 10.1038/ng.3245 [PubMed: 25751624]
5. Ferreira MA, et al. Identification of IL6R and chromosome 11q13.5 as risk loci for asthma. *Lancet*. 2011; 378:1006–1014. DOI: 10.1016/S0140-6736(11)60874-X [PubMed: 21907864]
6. Ferreira MA, et al. Shared genetic origin of asthma, hay fever and eczema elucidates allergic disease biology. *Nature genetics*. 2017; 49:1752–1757. DOI: 10.1038/ng.3985 [PubMed: 29083406]
7. Paternoster L, et al. Meta-analysis of genome-wide association studies identifies three new risk loci for atopic dermatitis. *Nat Genet*. 2011; 44:187–192. DOI: 10.1038/ng.1017 [PubMed: 22197932]
8. Roadmap Epigenomics C, et al. Integrative analysis of 111 reference human epigenomes. *Nature*. 2015; 518:317–330. DOI: 10.1038/nature14248 [PubMed: 25693563]
9. Sakaguchi S, Yamaguchi T, Nomura T, Ono M. Regulatory T cells and immune tolerance. *Cell*. 2008; 133:775–787. DOI: 10.1016/j.cell.2008.05.009 [PubMed: 18510923]
10. Josefowicz SZ, Lu LF, Rudensky AY. Regulatory T cells: mechanisms of differentiation and function. *Annu Rev Immunol*. 2012; 30:531–564. DOI: 10.1146/annurev.immunol.25.022106.141623 [PubMed: 22224781]
11. Kitagawa Y, et al. Guidance of regulatory T cell development by Satb1-dependent super-enhancer establishment. *Nat Immunol*. 2017; 18:173–183. DOI: 10.1038/ni.3646 [PubMed: 27992401]
12. Boschetti G, et al. Gut Inflammation in Mice Triggers Proliferation and Function of Mucosal Foxp3+ Regulatory T Cells but Impairs Their Conversion from CD4+ T Cells. *J Crohns Colitis*. 2017; 11:105–117. DOI: 10.1093/ecco-jcc/jlw125 [PubMed: 27364948]
13. Worthington JJ, et al. Integrin alphavbeta8-Mediated TGF-beta Activation by Effector Regulatory T Cells Is Essential for Suppression of T-Cell-Mediated Inflammation. *Immunity*. 2015; 42:903–915. DOI: 10.1016/j.jimmuni.2015.04.012 [PubMed: 25979421]
14. Tran, DQ; , et al. GARP (LRRC32) is essential for the surface expression of latent TGF-beta on platelets and activated FOXP3+ regulatory T cells. *Proceedings of the National Academy of Sciences of the United States of America*; 2009. 13445–13450.
15. Wang R, Wan Q, Kozhaya L, Fujii H, Unutmaz D. Identification of a regulatory T cell specific cell surface molecule that mediates suppressive signals and induces Foxp3 expression. *PloS one*. 2008; 3:e2705.doi: 10.1371/journal.pone.0002705 [PubMed: 18628982]
16. Dedobbeleer O, Stockis J, van der Woning B, Coulie PG, Lucas S. Cutting Edge: Active TGF-beta1 Released from GARP/TGF-beta1 Complexes on the Surface of Stimulated Human B Lymphocytes Increases Class-Switch Recombination and Production of IgA. *J Immunol*. 2017; 199:391–396. DOI: 10.4049/jimmunol.1601882 [PubMed: 28607112]
17. Wallace CH, et al. B lymphocytes confer immune tolerance via cell surface GARP-TGF-beta complex. *JCI insight*. 2018; 3doi: 10.1172/jci.insight.99863
18. Vermeersch E, et al. The role of platelet and endothelial GARP in thrombosis and hemostasis. *PloS one*. 2017; 12:e0173329.doi: 10.1371/journal.pone.0173329 [PubMed: 28278197]
19. O'Connor MN, et al. Functional genomics in zebrafish permits rapid characterization of novel platelet membrane proteins. *Blood*. 2009; 113:4754–4762. DOI: 10.1182/blood-2008-06-162693 [PubMed: 19109564]
20. Arvey A, et al. Genetic and epigenetic variation in the lineage specification of regulatory T cells. *eLife*. 2015; 4:e07571.doi: 10.7554/eLife.07571 [PubMed: 26510014]
21. Schmidl C, et al. The enhancer and promoter landscape of human regulatory and conventional T-cell subpopulations. *Blood*. 2014; 123:e68–78. DOI: 10.1182/blood-2013-02-486944 [PubMed: 24671953]
22. Oh H, et al. An NF-kappaB Transcription-Factor-Dependent Lineage-Specific Transcriptional Program Promotes Regulatory T Cell Identity and Function. *Immunity*. 2017; 47:450–465 e455. DOI: 10.1016/j.jimmuni.2017.08.010 [PubMed: 28889947]
23. Changelian PS, et al. Prevention of organ allograft rejection by a specific Janus kinase 3 inhibitor. *Science*. 2003; 302:875–878. DOI: 10.1126/science.1087061 [PubMed: 14593182]
24. Edwards JP, et al. Regulation of the expression of GARP/latent TGF-beta1 complexes on mouse T cells and their role in regulatory T cell and Th17 differentiation. *J Immunol*. 2013; 190:5506–5515. DOI: 10.4049/jimmunol.1300199 [PubMed: 23645881]

25. Eschborn M, et al. Activated glycoprotein A repetitions predominant (GARP)-expressing regulatory T cells inhibit allergen-induced intestinal inflammation in humanized mice. *J Allergy Clin Immunol.* 2015; 136:159–168. DOI: 10.1016/j.jaci.2015.04.020 [PubMed: 26145987]
26. Salem M, et al. GARP Dampens Cancer Immunity by Sustaining Function and Accumulation of Regulatory T Cells in the Colon. *Cancer Res.* 2019; 79:1178–1190. DOI: 10.1158/0008-5472.CAN-18-2623 [PubMed: 30674536]
27. Chen L, et al. Genetic Drivers of Epigenetic and Transcriptional Variation in Human Immune Cells. *Cell.* 2016; 167:1398–1414 e1324. DOI: 10.1016/j.cell.2016.10.026 [PubMed: 27863251]
28. Mumbach MR, et al. Enhancer connectome in primary human cells identifies target genes of disease-associated DNA elements. *Nature genetics.* 2017; 49:1602–1612. DOI: 10.1038/ng.3963 [PubMed: 28945252]
29. Rao SS, et al. A 3D map of the human genome at kilobase resolution reveals principles of chromatin looping. *Cell.* 2014; 159:1665–1680. DOI: 10.1016/j.cell.2014.11.021 [PubMed: 25497547]
30. Simeonov DR, et al. Discovery of stimulation-responsive immune enhancers with CRISPR activation. *Nature.* 2017; 549:111–115. DOI: 10.1038/nature23875 [PubMed: 28854172]

Methods References

1. Edwards JP, et al. Regulation of the expression of GARP/latent TGF-beta1 complexes on mouse T cells and their role in regulatory T cell and Th17 differentiation. *J Immunol.* 2013; 190:5506–5515. DOI: 10.4049/jimmunol.1300199 [PubMed: 23645881]
2. De Cuyper IM, et al. A novel flow cytometry-based platelet aggregation assay. *Blood.* 2013; 121:e70–80. DOI: 10.1182/blood-2012-06-437723 [PubMed: 23303822]
3. Asseman C, Mauze S, Leach MW, Coffman RL, Powrie F. An essential role for interleukin 10 in the function of regulatory T cells that inhibit intestinal inflammation. *The Journal of experimental medicine.* 1999; 190:995–1004. [PubMed: 10510089]
4. Picelli S, et al. Full-length RNA-seq from single cells using Smart-seq2. *Nature protocols.* 2014; 9:171–181. DOI: 10.1038/nprot.2014.006 [PubMed: 24385147]
5. Buenrostro JD, Giresi PG, Zaba LC, Chang HY, Greenleaf WJ. Transposition of native chromatin for fast and sensitive epigenomic profiling of open chromatin, DNA-binding proteins and nucleosome position. *Nat Methods.* 2013; 10:1213–1218. DOI: 10.1038/nmeth.2688 [PubMed: 24097267]
6. Pollard KS, Hubisz MJ, Rosenbloom KR, Siepel A. Detection of nonneutral substitution rates on mammalian phylogenies. *Genome Res.* 2010; 20:110–121. DOI: 10.1101/gr.097857.109 [PubMed: 19858363]
7. Browning BL, Zhou Y, Browning SR. A One-Penny Imputed Genome from Next-Generation Reference Panels. *Am J Hum Genet.* 2018; 103:338–348. DOI: 10.1016/j.ajhg.2018.07.015 [PubMed: 30100085]
8. Schmidl C, Rendeiro AF, Sheffield NC, Bock C. ChIPmentation: fast, robust, low-input ChIP-seq for histones and transcription factors. *Nat Methods.* 2015; 12:963–965. DOI: 10.1038/nmeth.3542 [PubMed: 26280331]
9. Zhang Y, et al. Model-based analysis of ChIP-Seq (MACS). *Genome Biol.* 2008; 9:R137.doi: 10.1186/gb-2008-9-9-r137 [PubMed: 18798982]
10. Liao Y, Smyth GK, Shi W. featureCounts: an efficient general purpose program for assigning sequence reads to genomic features. *Bioinformatics.* 2014; 30:923–930. DOI: 10.1093/bioinformatics/btt656 [PubMed: 24227677]
11. Delaneau O, et al. A complete tool set for molecular QTL discovery and analysis. *Nat Commun.* 2017; 8:15452.doi: 10.1038/ncomms15452 [PubMed: 28516912]
12. Giambartolomei C, et al. Bayesian test for colocalisation between pairs of genetic association studies using summary statistics. *PLoS Genet.* 2014; 10:e1004383.doi: 10.1371/journal.pgen.1004383 [PubMed: 24830394]
13. Bossini-Castillo L, et al. Immune disease variants modulate gene expression in regulatory CD4+ T cells and inform drug targets. *bioRxiv.* 2019

14. Rao SS, et al. A 3D map of the human genome at kilobase resolution reveals principles of chromatin looping. *Cell*. 2014; 159:1665–1680. DOI: 10.1016/j.cell.2014.11.021 [PubMed: 25497547]
15. Perez-Pinera P, et al. RNA-guided gene activation by CRISPR-Cas9-based transcription factors. *Nat Methods*. 2013; 10:973–976. DOI: 10.1038/nmeth.2600 [PubMed: 23892895]
16. Chen X, et al. Functional Interrogation of Primary Human T Cells via CRISPR Genetic Editing. *J Immunol*. 2018; 201:1586–1598. DOI: 10.4049/jimmunol.1701616 [PubMed: 30021769]

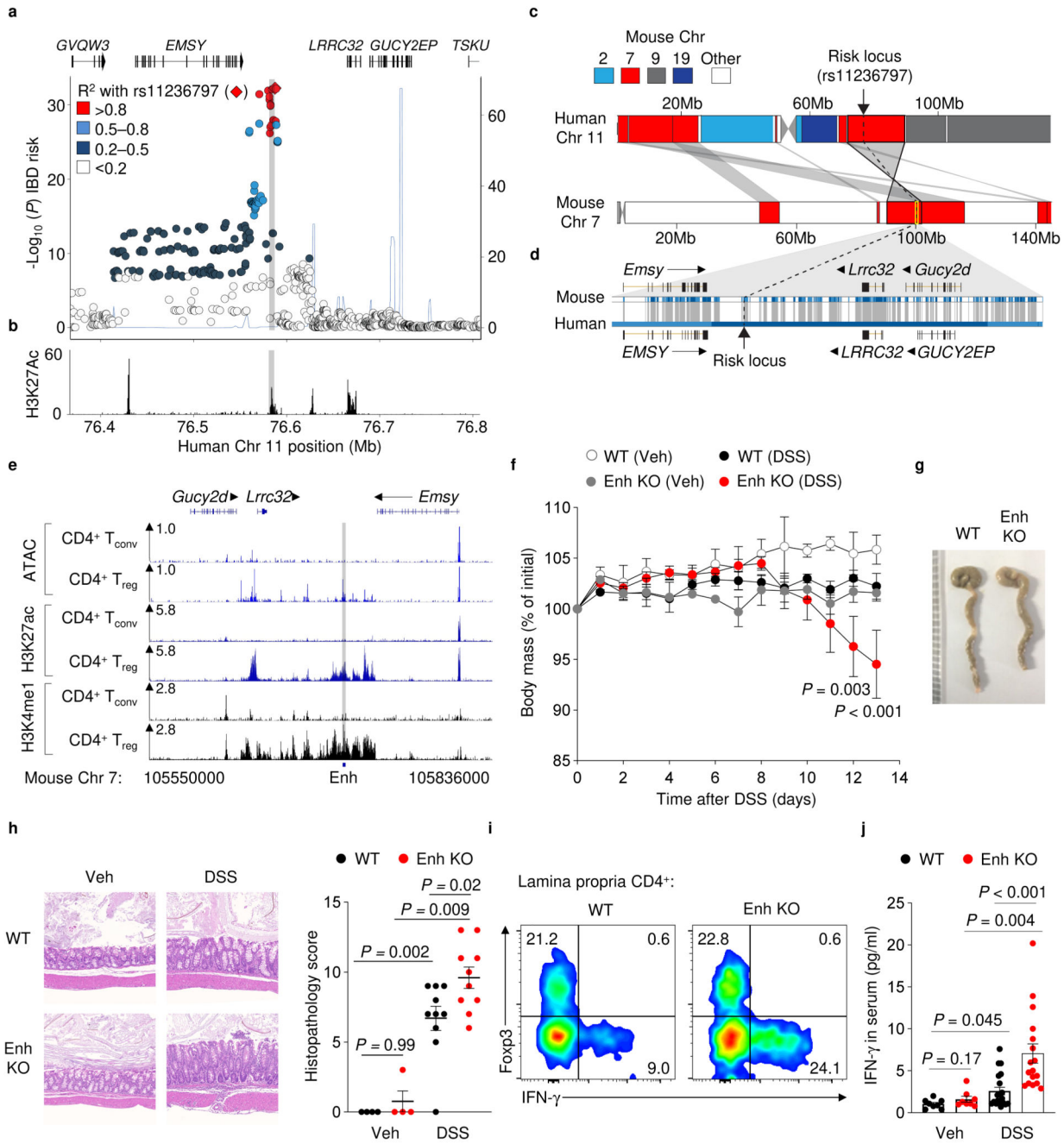


Figure 1. A distal intergenic region of mouse chromosome 7 in shared synteny with human 11q13.5 is required to limit gut inflammation.

a, Association of genetic polymorphisms at 11q13.5 with inflammatory bowel disease (IBD) risk (left axis; de Lange *et al.* for GWAS summary statistics and replicate information²). Imputed recombination rate (right axis; cM/Mb, CEU). Shaded area indicates polymorphic risk locus. Points represent individual single nucleotide polymorphisms (SNP; Minor allele frequency (MAF) threshold 0.01%). R² and MAF calculated using 2,686 genome sequences (UK10K). **b**, Alignment showing distribution of H3K27Ac at the indicated locus in human

CD4⁺ CD127⁻ CD25⁺ T_{reg} cells. Roadmap Epigenomics Project for sample information and replicate statistics⁸. **c**, Syntenic alignment of indicated human and mouse chromosomes. **d**, Gene-level alignment of mouse and human genome sequences containing identified risk locus. Grey regions, homology blocks; white spaces, non-aligned in mouse. **e**, Distribution of accessible chromatin (ATAC-Seq) and histone modifications in indicated T cell populations¹¹. Position of putative enhancer (Enh) within homology block containing risk SNP highlighted in grey. ATAC-Seq alignments representative of three independent biological replicates with samples isolated on different days. **f**, Mass of wildtype (WT) and enhancer-knockout (Enh-KO) mice administered dextran sulphate sodium (DSS) or vehicle (Veh). *P*, significance between daily WT and Enh-KO measurements within each treatment group; two-way ANOVA with Tukey's adjustment for multiple testing. $P > 0.05$, not shown. **g**, Representative photographs of large intestines 14 d after treatment initiation. **h**, Representative haematoxilin and eosin (H&E) staining (left) and combined histopathological colitis scores (right) of large intestines from animals in **g**. **i**, Representative flow cytometry of Foxp3 and IFN- γ expression by large intestinal lamina propria CD4⁺ T cells. **j**, Concentration of IFN- γ in the serum of animals in **g**. Representative of 3 (**f**) and 2 (**g-i**) independent experiments, or pooled from 2 independent experiments (**j**). $n=10$ and 4 mice per DSS- and Veh-treated group (**f**, **h**). $n=8$, 8, 20 and 17 for WT (Veh), Enh-KO (Veh), WT (DSS), Enh-KO (DSS) groups (**j**). Wilcoxon-Mann-Whitney test (**h**), unpaired two-tailed Student's *t* test (**j**). Bars and error show mean and s.e.m.

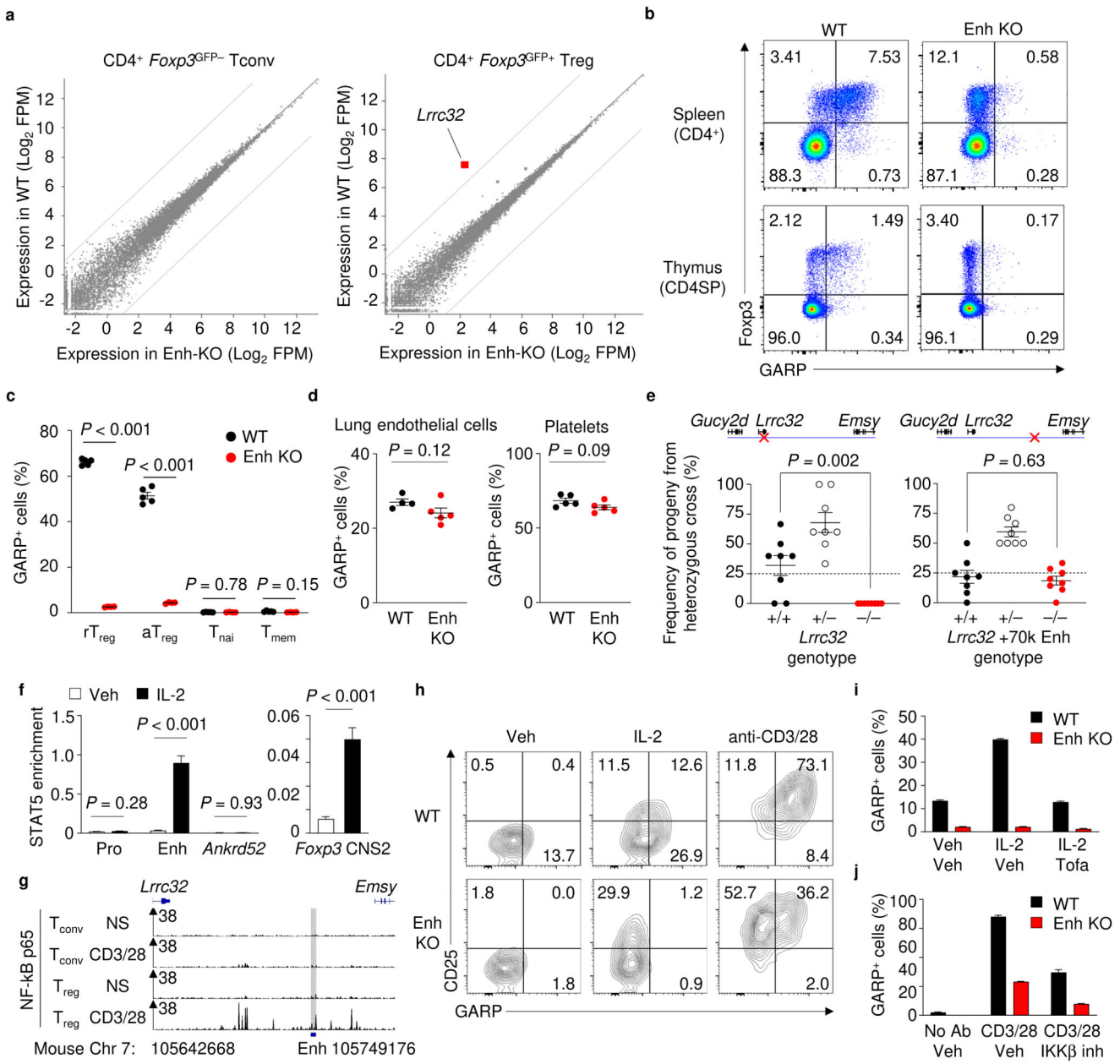


Figure 2. *Lrrc32* +70k is required for signal-driven expression of GARP by *Foxp3*⁺ T_{reg} cells.

a, Global differences in gene expression between WT and Enh-KO T_{conv} and T_{reg} cells (mean log₂ fragments per million (FPM) from 3 independent biological replicates, samples isolated on different days). Red dots indicate highly differentially expressed genes ($q < 0.05$, log₂ (FC) > 5 , mean FPM > 50). Two-tailed Wald test with Benjamini-Hochberg correction. **b**, Flow cytometry of GARP and Foxp3 expression by cells of indicated genotypes. CD4SP, CD4 single-positive. **c**, Frequency of GARP⁺ cells within indicated splenic CD4⁺ T cell populations. n=5 and 4 for WT and Enh-KO groups. Unpaired two-tailed Student's *t* test with Bonferroni correction. **d**, GARP expression on CD45⁻ CD31⁺ endothelial cells (left) and platelets following brief activation *ex vivo* (right); n=4 and 5 mice, WT and Enh-KO. **e**, Frequency of progeny from heterozygous crosses. **f**, ChIP-seq enrichment for STAT5 and Foxp3 CNS2. **g**, Genomic tracks for Lrrc32 and Emsy. **h**, Flow cytometry plots of CD25 vs GARP expression. **i**, Bar charts of GARP⁺ cell frequency under different conditions. **j**, Bar charts of GARP⁺ cell frequency under different conditions.

n=5 mice per group). **e**, Frequency of progeny genotypes after mating of mice heterozygous for the *Lrrc32* KO (left) or *Lrrc32*+70k Enh-KO alleles (right). Horizontal line indicates expected Mendelian frequency of homozygous offspring. n=8 litters per allele from independent matings. **f**, Input-normalised STAT5 ChIP-PCR enrichment at the indicated loci. **g**, NF-κB p65 binding in the indicated cell types with or without TCR stimulation. Oh *et al.* for sample information and replicate statistics²². **h**, CD25 and GARP expression on CD4⁺ Foxp3⁺ T_{reg} cells cultured under indicated conditions for 16 h *in vitro*. **i-j**, Frequency of GARP⁺ cells on Foxp3⁺ T_{reg} cells following stimulation with IL-2 with or without pre-treatment with the JAK inhibitor Tofacitinib (Tofa; **i**) or with anti-CD3/28 antibodies with or without pre-treatment with an IKKβ inhibitor (IKKβ inh; **j**). Data shows 3 (**f**) or 4 (**i-j**) technical replicates per condition. Data are representative of 5 (**b**) and 2 (**c-d, g-j**) independent experiments or pooled from 2 independent experiments (**f**). Unpaired two-tailed Student's *t* test (**d-f**). Bars and error show mean and s.e.m.

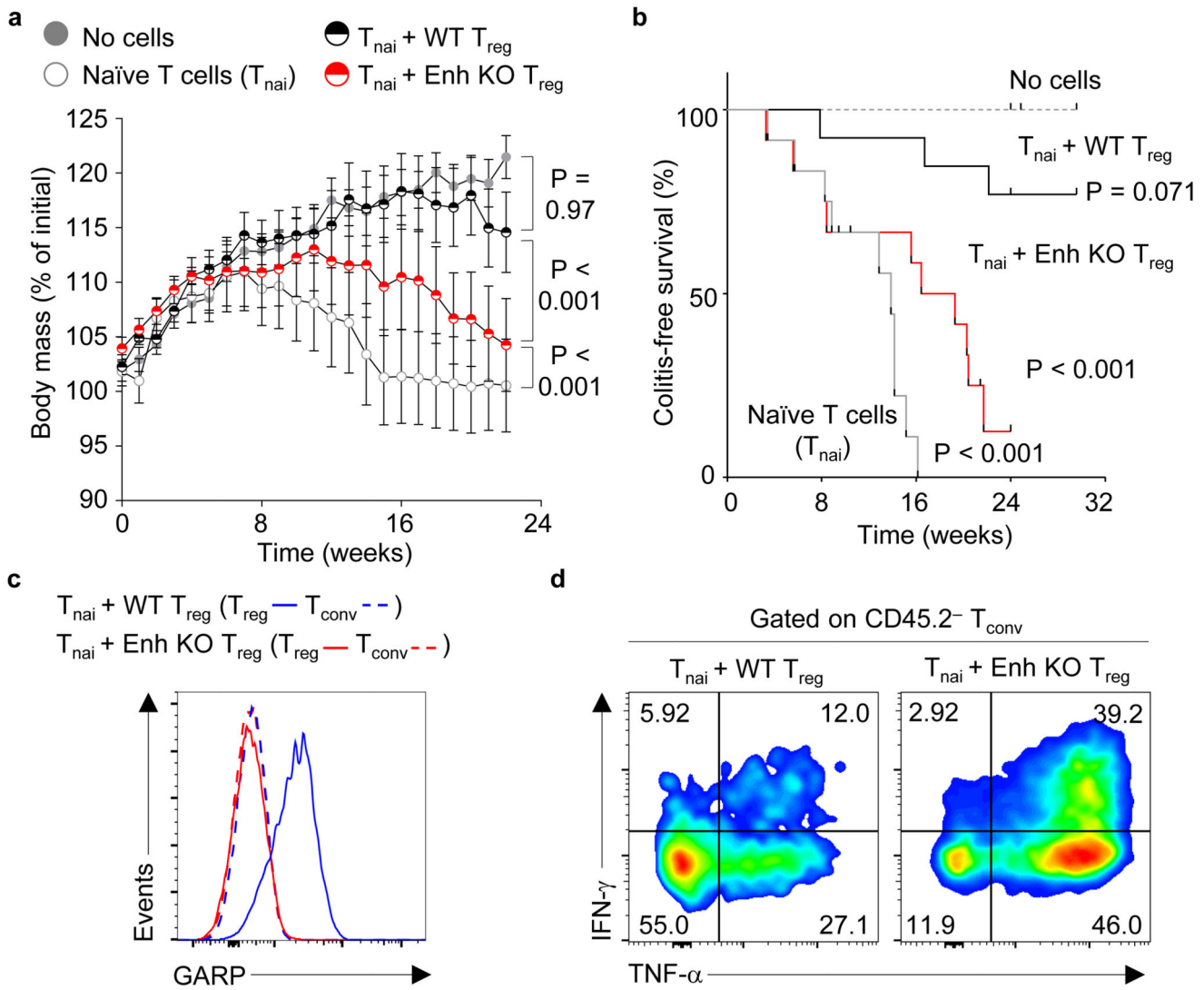


Figure 3. *Lrrc32 +70k* promotes T_{reg} -mediated suppression of colitis.

a-b, Body mass (**a**) and colitis-free survival (**b**) of *Rag2*-deficient animals injected with WT naïve $CD4^+ CD25^- CD45RB^{high}$ T cells alone (T_{nai} ; n=12), or in combination with $CD4^+ CD25^{high}$ T_{reg} cells derived from WT (n=13) or Enh-KO (n=12) animals. Control animals did not receive cells (n=10). **c**, GARP expression gated on indicated cells from mLN of mice euthanized 100 d following reconstitution. T_{reg} , $CD45.2^+$ cells; T_{conv} , $CD45.2^-$ cells. **d**, Representative flow cytometry of expression of indicated cytokines by $CD45.2^-$ cells from mLN following brief restimulation *ex vivo*. Pooled results from two independent experiments (**a-b**). Data representative of 2 independent experiments (**c-d**). 2-way ANOVA with Tukey's correction for multiple comparisons (**a**) and Mantel-Cox log-rank test (**b**). Bars and error show mean and s.e.m.

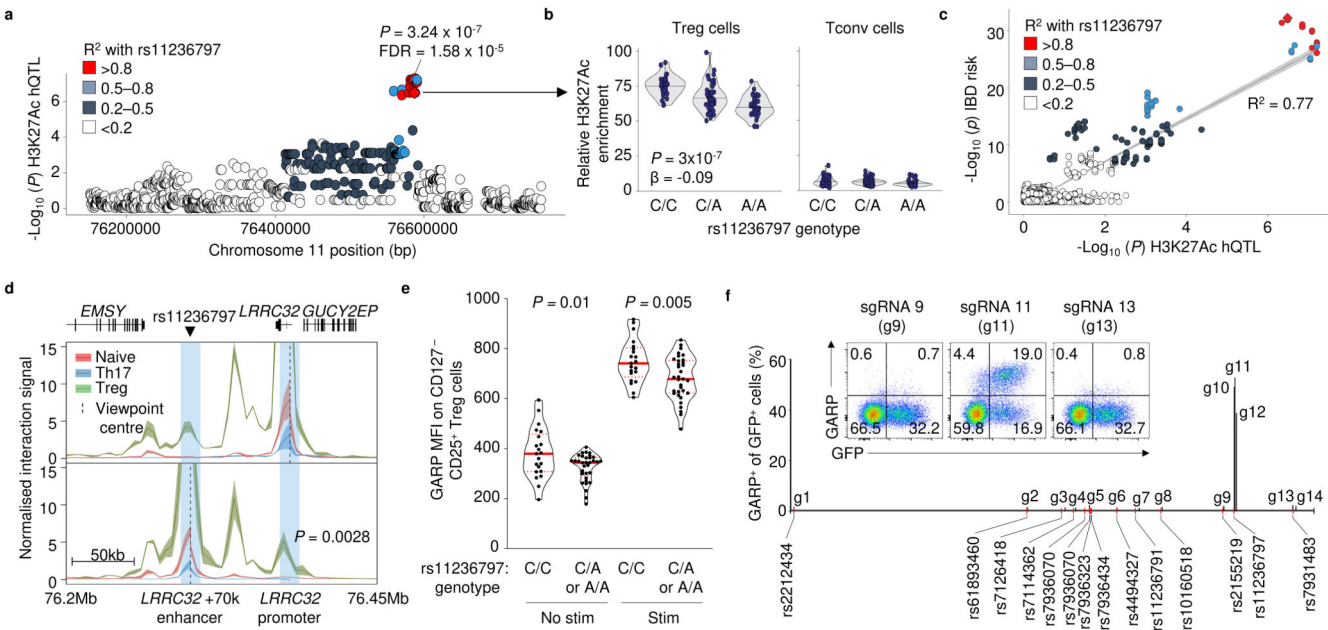


Figure 4. Inflammatory bowel disease risk alleles at 11q13.5 affect enhancer histone acetylation and GARP expression in human CD4⁺ Treg cells.

a, Histone quantitative trait locus (hQTL) analysis of the association between indicated SNP (points) and histone H3K27Ac enrichment at the identified enhancer at chr11:76586431-76600121 in human CD4⁺ CD127⁻ CD25⁺ T_{reg} cells; n=91 donors. Nominal p and false discovery rate (FDR) of most significantly associated SNP shown. **b**, Association of rs11236797 polymorphisms with H3K27Ac enrichment at chr11:76586431-76600121 in human T_{reg} and CD4⁺ T_{conv} cells²⁷; n=91 donors. **c**, Co-localisation of the association of indicated SNP with H3K27ac enrichment (x -axis) and IBD risk (y -axis). Co-localisation posterior probability=0.97; n=91 donors. **d**, Reciprocal v4C analysis of H3K27Ac-enriched HiChIP interactions within human CD4⁺ naïve, T_{reg}, and Th17 cells²⁸. Graph lines and shaded area show mean and s.e.m; n=3 biological replicates. **e**, GARP MFI on CD127⁻ CD25⁺ T_{reg} cells from donors of indicated genotypes stimulated with anti-CD3/28 and IL-2 or media alone. n=21 (C/C) and 33 (C/A or A/A) donors. **f**, GARP expression on human GFP⁺ (transduced) CD4⁺ T cells expressing sgRNAs targeting VP64-dCas9 to loci indicated by the x -axis position of bars. Positions of risk SNP are shown. Representative of three independent experiments using cells from three different donors. Linear regression, two-sided (a-c), unpaired two-tailed Student's t test (d, e). Violin plot lines and outlines show mean and frequency distribution.